JGR Atmospheres

RESEARCH ARTICLE
10.1029/2022JD037107

Effect of Marine and Land Convection on Wet Scavenging of Ozone Precursors Observed During a SEAC^{4}RS Case Study

G. C. Cuchiara[1,2,3], A. Fried[1], M. C. Barth[2], M. M. Bela[4,5], C. R. Homeyer[6], J. Walega[1], P. Weibring[1], D. Richter[1], S. Woods[7], A. Beyersdorf[8,9], T. V. Bui[10], and J. Dean-Day[10]

[1]Institute of Arctic and Alpine Research, University of Colorado, Boulder, CO, USA, [2]Atmospheric Chemistry Observations and Modeling Laboratory, National Center for Atmospheric Research, Boulder, CO, USA, [3]Now at Cooperative Institute for Research in the Atmosphere, Colorado State University, Fort Collins, CO, USA, [4]Cooperative Institute for Research in Environmental Sciences, University of Colorado Boulder, Boulder, CO, USA, [5]Chemical Sciences Laboratory, Earth System Research Laboratory, NOAA, Boulder, CO, USA, [6]School of Meteorology, University of Oklahoma, Norman, OK, USA, [7]Stratton Park Engineering Company, Inc., Boulder, CO, USA, [8]Chemistry and Dynamics Branch, Langley Research Center, National Aeronautics and Space Administration, Hampton, VA, USA, [9]Chemistry Department, California State University, San Bernardino, CA, USA, [10]Ames Research Center, Bay Area Environmental Research Institute, National Aeronautics, and Space Administration, Moffett Field, CA, USA

Key Points:

- Although marine and land convection have different microphysical properties, there are no relevant differences in the scavenging efficiency
- WRF-Chem simulations analysis shows ice retention factor for formaldehyde is higher than found in previous studies
- Methyl hydrogen peroxide scavenging efficiencies are higher than expected from Henry's Law, even with potential measurement interference

Supporting Information:

Supporting Information may be found in the online version of this article.

Correspondence to:

G. C. Cuchiara,
cuchiara@colostate.edu

Citation:

Cuchiara, G. C., Fried, A., Barth, M. C., Bela, M. M., Homeyer, C. R., Walega, J., et al. (2023). Effect of marine and land convection on wet scavenging of ozone precursors observed during a SEAC^{4}RS case study. *Journal of Geophysical Research: Atmospheres*, *128*, e2022JD037107. https://doi.org/10.1029/2022JD037107

Received 12 MAY 2022
Accepted 20 JAN 2023

Abstract

Convective clouds are important for both the vertical redistribution of tropospheric trace gases and the removal, via microphysical scavenging, of soluble trace gas precursors of ozone. We investigate wet scavenging of formaldehyde (CH_2O), hydrogen peroxide (H_2O_2), and methyl hydrogen peroxide (CH_3OOH) in quasi-marine and land convective storms over Texas, USA observed on 18 September 2013 during the 2013 SEAC^{4}RS campaign. Cloud-resolving simulations using the Weather Research and Forecasting model with Chemistry (WRF-Chem) were performed to understand the effect of entrainment, scavenging efficiency (SE), and ice physics processes on these trace gases with varying solubility. While marine and land convection can have distinctly different microphysical properties, we did not find significant differences in the SEs of CH_2O, H_2O_2, or CH_3OOH. The SEs of 44%–53% for CH_2O and 85%–90% for H_2O_2 are consistent with our previous studies from SEAC^{4}RS and the 2012 DC3 field experiment storms. Using WRF-Chem simulations, the ice retention factor (r_f) for CH_2O was determined to be 0.5–0.9, which is higher than found in previous studies. We show that the CH_2O r_f is higher in airmass and multicell storms than in severe storms and hypothesize that ice shattering may affect CH_2O r_f values. The CH_3OOH SEs (39%–73%) were higher than expected from Henry's Law equilibrium. While recent studies suggest that CH_3OOH measurements have interference due to methane diol, we find that this interference cannot fully explain the higher-than-expected CH_3OOH SEs determined here and during DC3, suggesting further research is needed to understand CH_3OOH vertical redistribution.

Plain Language Summary

Thunderstorms are important mechanisms for the transport and removal of trace gases in the atmosphere. This study investigates the transport and removal processes of tropospheric ozone trace gas precursors in marine and land convective storms over Texas, USA. Numerical simulations were performed to understand storm processes affecting atmospheric gases with different solubilities. While marine and land storms can have distinctly different storm structure and updraft winds, we did not find significant differences in the amount of gases removed by these storms. The results show that the efficiency of the storm in removing gas from the atmosphere is consistent with our previous findings for moderate to severe storms over the US. In addition, the analysis showed when cloud drops freeze onto ice and snow particles that formaldehyde had more retention in the frozen particle in moderate storms compared to severe storms suggesting that there are many processes affecting this key ozone precursor in deep convection. The more soluble hydrogen peroxide did not show the same ice retention behavior because it is removed by precipitation in the warmer, liquid-only region of the storm.

1. Introduction

Convective storms play an important role in the vertical transport of pollutants as they are efficient mechanisms for transporting planetary boundary layer (PBL) constituents to the upper troposphere (UT—Dickerson et al., 1987). During the convectively-driven transport, soluble trace gases and aerosols interact with cloud physics (precipitation, ice deposition, entrainment, etc.) with only a fraction of the pollutants deposited in the

mid/upper troposphere by the thunderstorm. Depending on the UT environment and the gas/aerosol content of the plume being transported, secondary production of pollutants such as ozone (O_3) and aerosols can occur in the UT (Clarke, 1993; Pickering et al., 1992; Radke & Hobbs, 1991; Thompson et al., 1994; Twohy et al., 2002). Thus, convective transport of trace gases to the UT via thunderstorms can impact the chemical composition of the UT and lower stratosphere as well as the Earth's radiation budget (Martini et al., 2011). Therefore, the quantification of the fraction of each of these soluble constituents reaching the UTLS of the atmosphere, or conversely their scavenging efficiencies (SEs), is ultimately needed to fully understand the vertical transport of constituents and their long-term impact on Earth's atmosphere.

Studies from the 2012 Deep Convective Clouds and Chemistry Project (DC3—Barth et al., 2015) and the 2013 Studies of Emissions, Atmospheric Composition, Clouds and Climate Coupling by Regional Surveys (SEAC^{4}RS—Toon et al., 2016) airborne campaigns calculated a range of SEs of three important trace gases with different Henry's Law solubilities that are precursors of O_3: hydrogen peroxide (H_2O_2– $K_H(H_2O_2) = 2.7 \times 10^5$ M atm^{-1} at 285 K), a highly soluble trace gas; formaldehyde (CH_2O–$K_H(CH_2O) = 9.6 \times 10^3$ M atm^{-1} at 285 K), a moderately soluble trace gas, and methyl hydrogen peroxide (CH_3OOH–$K_H(CH_3OOH) = 670$ M atm^{-1} at 285 K), a low solubility trace gas. During the 2012 DC3 study, Fried et al. (2016) reported remarkably consistent CH_2O SEs employing various approaches for four storms studied on 29 May (SE = 54% ± 3%), 6 June (SE = 54% ± 6%), 11 June (SE = 58% ± 13%), and 22 June (41 ± 4%). It is noteworthy that this consistency spans a large geographic region of the United States (northeast Colorado, central Oklahoma, southern Missouri, northern Alabama, Mississippi, and Arkansas) with different types of strong convection (including severe and a mesoscale convective systems), differences in measured ice water content between storms, vastly different boundary layer compositions, and differences in biogenic activity (low biogenic activity in the Colorado region compared to the other regions). Likewise, the reported CH_2O SEs for airmass and multicellular storms studied on 2 September 2013 during the SEAC^{4}RS campaign over Mississippi revealed nearly identical results of 47% ± 8% and 50 ± 6%, respectively, after accounting for the production of CH_2O from chemistry affected by lightning-generated nitrogen oxides (Cuchiara et al., 2020). This consistency in the SE for CH_2O for these various storms is noteworthy given that previous studies before DC3 exhibited a much wider range from 4% to 78% (Fried et al., 2016 and references therein). More recently, Bozem et al. (2017) deduced CH_2O SEs of 0%–47% for a deep convection case study over Germany during the HOOVER II project. The upper end of this range agrees with the DC3 results but the values near 0 are more consistent with the Borbon et al. (2013) values ranging between 4% and 39% for various storms.

In the case of H_2O_2, Barth et al. (2016) report SEs of 79%–97% with relative uncertainties of 5%–25% during DC3. These values are consistent with SEAC^{4}RS values of 80%–90% for the two different storm types (Cuchiara et al., 2020). In contrast, Bozem et al. (2017) determined H_2O_2 SEs of 32%–41% during the HOOVER II project, a range significantly lower than DC3. Bozem et al. (2017) suggest the possibility that H_2O_2 may degass from cloud droplets during freezing, thus reducing its SE. Presumably this same process will also lead to lower CH_2O SEs, but this was not addressed in the Bozem et al. (2017) study. Thus, given the potential importance of ice degassing and its effect on SE, we provide in the present study estimates for the ice retention factors for CH_2O, H_2O_2, and CH_3OOH in addition to SE determinations.

The SE for CH_3OOH was generally smaller in the SEAC^{4}RS airmass and multicell storms (4%–27%; Cuchiara et al., 2020) compared to DC3 severe convection (12%–84%, Barth et al., 2016) suggesting that perhaps other processes, for example, trace gas and cloud physics interactions and multiphase chemistry, may affect CH_3OOH mixing ratios within the convection. Using WRF-Chem simulations, Bela et al. (2018) found that the higher CH_3OOH SEs may be due to the fraction of CH_3OOH retained in frozen particles as cloud drops freeze. Cuchiara et al. (2020) provided evidence that changes in gas-phase chemistry must also be considered due to NO_x ($NO + NO_2$) production from lightning, which can enhance CH_2O production and reduce H_2O_2 and CH_3OOH production. While the surprisingly high variance in CH_3OOH SE results could be due to other physical or chemical processes, one cannot rule out two potential measurement issues that may affect the CH_3OOH SE results. These potential measurement issues will be discussed later in this paper.

The interaction between cloud physics and trace gases has been investigated in past years, but due to its complexity, there are still open questions, especially related to the interaction between ice crystal formation and various trace gases during hydrometeor freezing. While air masses ascend in the convective updraft, the dissolution of gases like CH_2O and H_2O_2, for example, could be significantly impacted as droplets freeze onto the ice, snow, and graupel particles. Results from a cloud chemistry model intercomparison study (Barth, Kim, Wang,

et al., 2007) showed that models with different cloud microphysics parameterizations and assumptions about ice retention produced varying results for CH_2O, H_2O_2, and HNO_3 in convective outflows. In chemistry transport models, a parameter called the ice retention factor (*rf* = fraction of trace gas retained in an ice particle when cloud drops freeze), which ranges in value from 0 to 1, is used to adjust the trace gas partitioning between gas and condensed phases in the presence of ice. In the case of CH_2O, many authors have investigated phase partitioning during liquid-to-solid freezing and riming to better understand and represent these effects (Jost et al., 2017; Leriche et al., 2013; Snider & Huang, 1998; Stuart & Jacobson, 2004, 2006; Voisin et al., 2000; von Blohn et al., 2011, 2013), but there is a large range of reported *rf* values, which can create uncertainties in model predictions of convective transport of HO_x ($OH + HO_2$) precursors and subsequent O_3 chemistry. The discrepancies among these different studies highlight the importance of further examining SE and *rf* for soluble trace gases for different storm types.

Previous studies examining SE and *rf* relationships (Bela et al., 2018; Cuchiara et al., 2020) investigated convective storms that occurred exclusively over land. This study analyzes data acquired on 18 September 2013, during the SEAC^{4}RS field study where both marine and land convection were sampled in the same south-east flow, providing the opportunity to further examine the relationship between SE and *rf* in different environments. Marine and land convection develop in distinct thermodynamic environments resulting in different microphysical characteristics. Marine convection generally has fewer cloud condensation nuclei (CCN) of 30–200 cm^{-3} (Clarke & Kapustin, 2010; Moore et al., 2013) than land convection (CCN 500–5,000 cm^{-3}), while ice-forming nuclei span a wide range of concentrations in both marine and land regions (0.02–200 L^{-1}; Demott et al., 2010). Lucas et al. (1994) investigated aircraft-measured vertical velocities within deep convection over the ocean and continental air masses and found similar Convective Available Potential Energy (CAPE) between the two environments, yet convective updraft cores of maritime systems are only one-third or one-half the size of those of land systems. Williams and Stanfill (2002) found that cloud physics and dynamics contrast between marine and land convection resulting in different cloud-base heights. Generally, marine environments have a smaller surface sensible-to-latent heat flux ratio (~0.1) compared to land environments (0.2–1), higher relative humidity (~80%) compared to values of 20%–60% over land, and a lower and warmer cloud-base height (~500 m) compared to those over land where the cloud base typically ranges between 1—4 km. These marine environment characteristics tend to enhance warm rain processes, create weaker updrafts, and suppress supercooled water in deep convection. All these differences can lead to different cloud physics processes, which dominate precipitation formation and hence impact the scavenging of soluble trace gases. Thus, the September 18th SEAC^{4}RS data set provides a unique opportunity to examine differences in SEs and *rf* in marine convection compared to land convection as well as expand our database of SEs for O_3 precursors.

Similar to the analysis of Cuchiara et al. (2020) for the September 2nd SEAC^{4}RS case study, the present work combines both observational techniques and modeling approaches in studying wet scavenging processes in convection for various storm intercepts on 18 September 2013 over the Gulf of Mexico and Texas during the SEAC^{4}RS campaign. SEs and *rf*s for marine convection are discussed in the context of previous studies of a variety of storm types over land. The results from this study highlight that a single *rf* used in modeling parameterizations may not be adequate. We also discuss potential measurement uncertainties that may explain the large range of CH_3OOH SEs observed in previous studies.

2. Case Study Description and Data

As part of the analysis, we compare the results for the 18 September 2013 case study with storms that we have analyzed previously. The different storms discussed in this paper are listed in Table S1 in Supporting Information S1. Two storms that occurred near Jackson, MS on 2 September 2013 during SEAC^{4}RS and several storms from the DC3 field campaign are included in the discussion of results. The DC3 storms were generally more severe than those sampled during SEAC^{4}RS and occurred in the central US.

2.1. Overview of September 18th Storm Cases

This study uses data from the National Aeronautics and Space Administration (NASA) DC-8 aircraft collected during the SEAC^{4}RS field campaign to analyze both marine and land convection sampled on 18 September 2013 (Figure 1). The 1-s DC-8 aircraft merged data is used in this work. The near-surface synoptic environment in

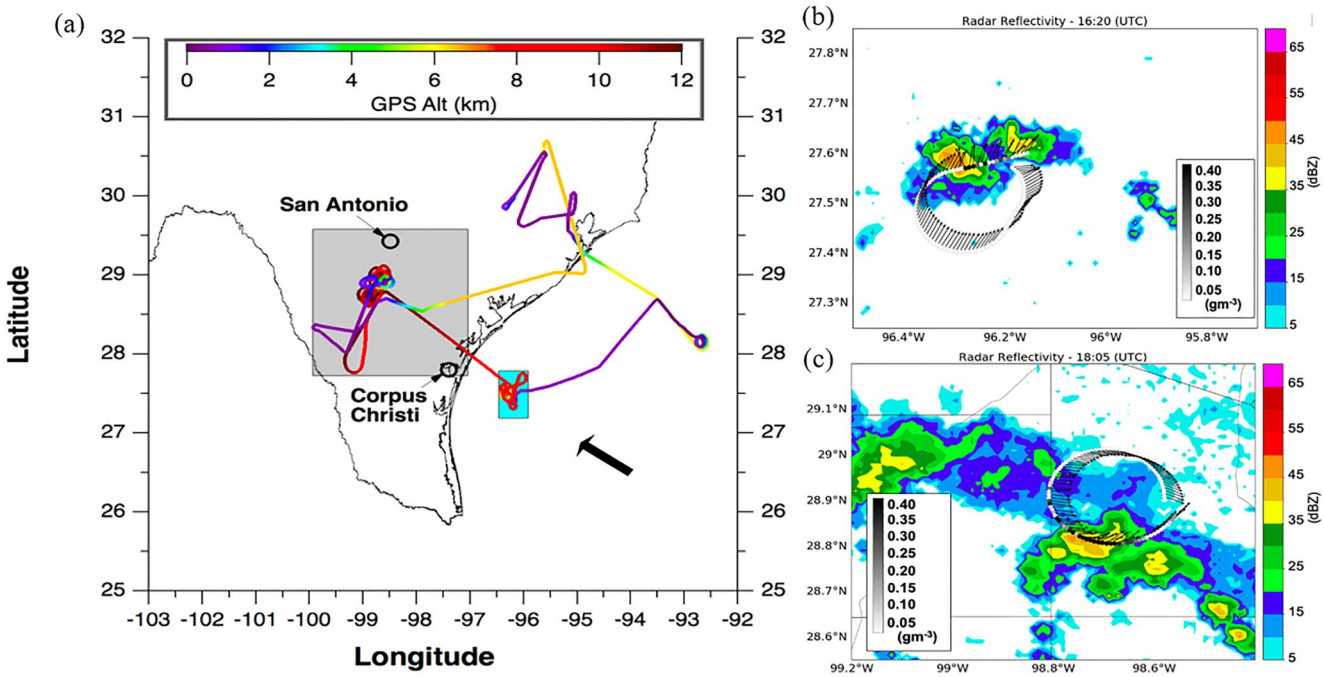

Figure 1. (a) DC-8 flight track for SEAC[4]RS 18 September case. Radar reflectivity (b) at ∼8 km in the marine storm at 16:20 UTC, and (c) at ∼10 km in the land storm at 18:05 UTC. The flight tracks in (b and c) are colored by IWC (g m^{-3}) overlaid on Next Generation Weather Radar composite radar imagery (dBZ). The land study area box (gray square in a) is defined by the coordinates (Latitude: 27.727°N–29.580°N, Longtitude: 97.042°W–99.939°W), and the marine study area box (blue square in a) is defined by the coordinates (Latitude: 27.150°N–27.450°N, Long: 95.450°W–96.450°W). Arrows in (a) show points of reference in the map and arrows in (b and c) represent the direction of the wind. The synoptic on-shore wind is displayed by the large arrow in (a). For display purposes, IWC and wind measurements are presented in a 3-s interval in (b and c).

southern Texas (Figure S1 in Supporting Information S1) was influenced by the position of a high-pressure system centered over the Washington D.C. region, extending over much of the Southeast U.S. This is a semi-permanent high-pressure system also known as "Bermuda High" as its preferable position during the summer months is over the Atlantic Ocean. In the late summer and early fall of 18 September 2013, this high-pressure system was spatially displaced westward of its favorable position such that the clockwise circulation impacted the entire south-eastern portion of the continental U.S. including the coast of Texas. The position of the high-pressure system was related to two low-pressure systems: one over the Yucatan peninsula and the other an evolving tropical system (Miguel) on the west coast of Mexico, which favored a southeasterly flow transporting moisture from the Gulf of Mexico toward the land where the air temperatures over the southern portion of the Texas coast were elevated (30–35°C). This synoptic condition allowed the generation of moderate instability at the marine-land interface where low convection inhibition (CIN = 6.4 J) and moderate CAPE (2400 J kg^{-1}) were observed approximately three hours before the sampling period (12 UTC) at the Corpus Christi, TX (Figure 1a; CRP—27.76°S; −97.50°W) ground-based radar sampling site.

The DC-8 approached the region at ∼15:30 UTC and began sampling the marine boundary layer atmosphere depicted in Figure 1a (cyan box) before performing vertical spirals where mainly three clouds were sampled in the cluster of widespread convection. At ∼16:00 UTC, the airplane intercepted one convective cell over the Gulf (Figure 1b and Figure S2a in Supporting Information S1), performing five consecutive intercepts in 1 hour. After sampling the marine environment, the DC-8 aircraft headed inland to intercept two convective cells that developed over the continental region southwest of San Antonio, TX (Figure 1c and Figure S2b in Supporting Information S1). Twelve intercepts (Table S1 in Supporting Information S1) were sampled in a little over an hour.

Lawson et al. (2017) examined the cloud structure of the SEAC[4]RS September 18th case, among other campaigns and locations, using data from the Stratton Park Engineering Company Incorporated (SPEC) Lear jet to determine any relationships between cloud-base temperature, drop size distribution, and the development of supercooled water drops and ice in strong updraft cores of convective clouds. They classified the environment where these clouds developed as "quasi maritime" because the drop size distribution near the cloud base is relatively

broad, but CCN concentration and total drop concentration are higher than expected in a maritime environment (Hudson, 1993). The large observed CCN concentration is likely due to the proximity of urban coastal areas, heavy ship traffic, and numerous offshore oil rigs. Although Lawson et al. (2017) classified both the Gulf of Mexico and the southwest of San Antonio convective cell as developing in the same "quasi marine environment," the approach proposed on this work will analyze these intercepts individually. The CCN concentrations measured in the inflow of the marine storm (282 cm^{-3}) were almost half of the value measured in the inflow of the storm over land (484 cm^{-3}) for both this September 18th case (Figure S3 in Supporting Information S1) as well as the previously studied SEAC^{4}RS September 2nd land convection (533 cm^{-3}) airmass and multicell storms over Mississippi. The mean cloud-base updraft velocities measured were 0.9 m s^{-1} over land and 0.3 m s^{-1} over water in the Gulf Coast of Mexico, and the average observed velocity in Gulf cloud updraft cores within the temperature range of 11.5°C–4.6°C was 5.3 m s^{-1} (Lawson et al., 2017). The NASA DC-8 aircraft sampled three convective clouds (Table S1 in Supporting Information S1). The liquid water content (LWC) in the low altitude intercept in the marine convection (0.50 ± 0.24 g kg^{-1}) is higher than the land convection (0.18 ± 0.25 g kg^{-1}) on 2 September 2013 (Cuchiara et al., 2020). The cloud base was measured at ∼600 m of altitude, which is approximately two times lower than the 2 September cloud base altitude of ∼1,400 m (Lawson et al., 2017). The PBL height over the Gulf of Mexico was observed at ∼600 m while the land PBL heights were observed at ∼1,500 m.

Lawson et al. (2017) found a concentration of supercooled drops ≥1 mm in diameter of 332 m^{-3} at 1–3 km above cloud base, which is lower in concentration compared to measurements from the Caribbean marine environment (1,015 m^{-3}) during the Clouds Experiment–Tropical field project but higher compared to those found in the Southeast United States (198 m^{-3}) during SEAC^{4}RS. In addition, an analysis of DC-8 and Learjet data shows that supercooled liquid water was detectable as cold as −21°C over both the Gulf and over the Southeast United States. It is important to note that although the marine environment is characterized by a coastal area impacted by anthropogenic activities, as mentioned earlier, we will refer to this case simply as marine from now on. Similarly, the proximity of the land convection to the marine environment and the direction of the wind flow could characterize this case as a coastal-continental. Regardless, the marine convection sampled on 18 September 2013 has different physical properties than the land convection, allowing us to investigate the differences in the SEs of soluble trace gases between marine and land convection.

2.2. Data and Modeling Methods

Several airborne in situ instruments were used to measure the atmospheric microphysical, dynamical, and chemical properties during SEAC^{4}RS. This work utilizes meteorology (vertical profiles of temperature, dew-point temperature, and winds), cloud properties (radar reflectivity, vertical velocities, CCN, ice water content IWC, and LWC), and chemical composition (CH_2O, H_2O_2, CH_3OOH, carbon monoxide (CO), and carbon dioxide (CO_2)) observations collected aboard the NASA DC-8 airplane during the SEAC^{4}RS campaign to quantify and estimate scavenging processes impacting trace gas distributions during convection, such as entrainment, SE, precipitation production, ice retention, and chemical transformations.

The Meteorological Measurement System (MMS; Chan et al., 1998) provided air temperature and flight-level three-dimensional winds with 0.1 m s^{-1} precision for the vertical velocity measurements. The SPEC High Volume Precipitation Spectrometer version 3 (HVPS-3; Lawson et al., 1998) measured IWC based on particle sizes ranging from 150 to 19,200 microns and the 2D-S (Stereo) Optical Array Cloud Particle Imaging Probe provided measurements based on particle sizes ranging from 10 μm to 3 mm (Lawson, 2011). The Airborne Precipitation Radar version 2 (APR-2; Sadowy et al., 2003), which is a dual-frequency (13 and 35 GHz) dual-polarization Doppler radar system aboard the DC-8, aided the identification of cloud characteristics. Radar, ground measurements, and sounding data were utilized to compare the surrounding thermodynamics environment and the dynamical and microphysical properties of the storms to also evaluate the performance of the model storm simulation. Next Generation Weather Radar (NEXRAD) reflectivity was used to identify cloud cells and general periods when the DC-8 intercepted cloud cores.

Measurements of CH_2O, H_2O_2, and CH_3OOH employed in this analysis have been discussed in more detail by Cuchiara et al. (2020) and we present here a summary. The CH_2O measurements 1-s merged data were collected by two instruments during SEAC^{4}RS flights: the University of Colorado Compact Atmospheric Multispecies Spectrometer (CAMS; Richter et al., 2015) and the NASA Goddard Space Flight Center In situ Airborne Formaldehyde (ISAF; Cazorla et al., 2015) system. A combined data set was first derived based on 10-s averages by

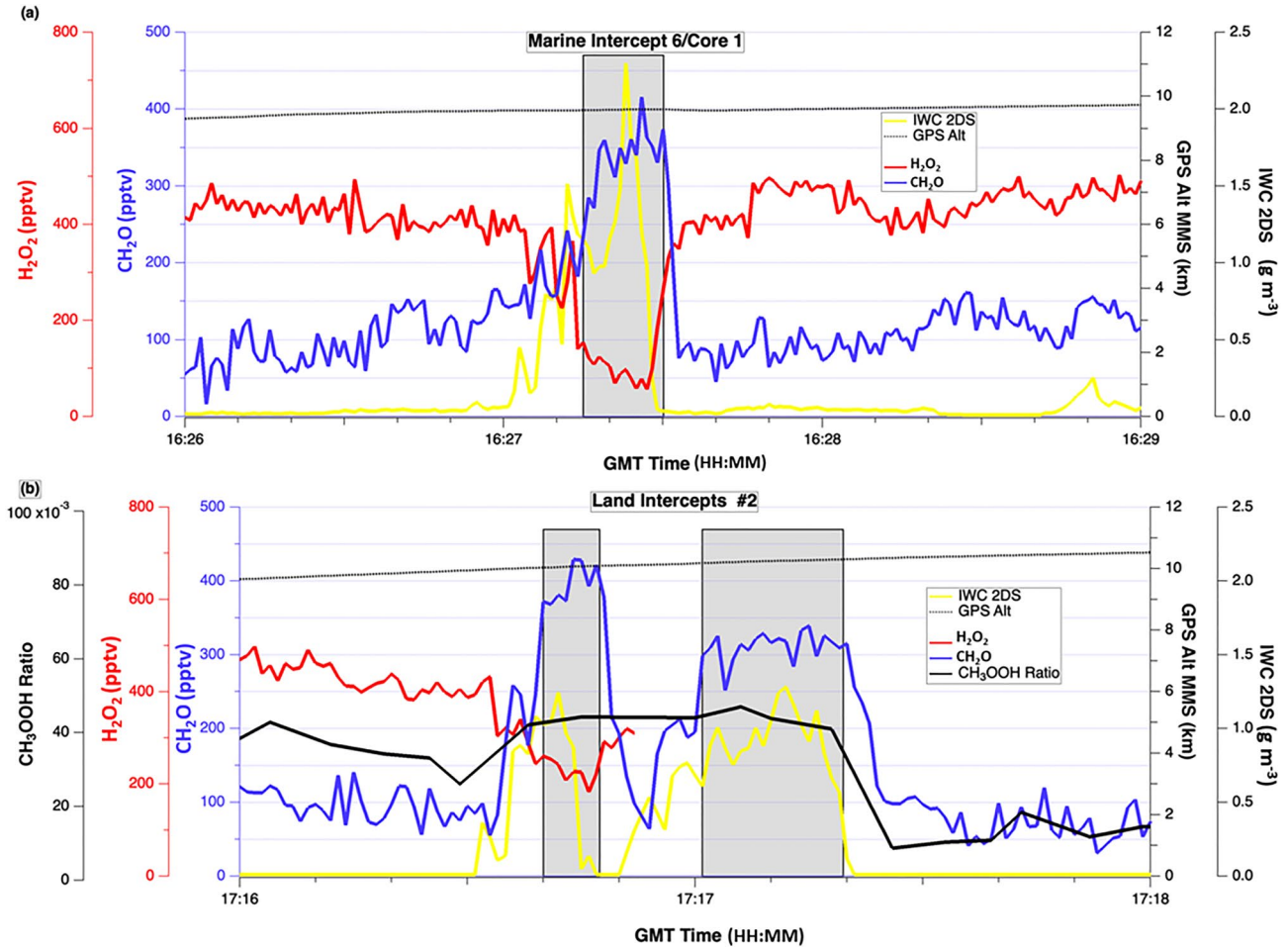

Figure 2. Time series of storm core intercept for (a) marine convection at 16:27 UTC and (b) land convection at 17:17 UTC on 18 September 2013, with the IWC expressed in g m^{-3}. Note that the CH_3OOH ratios are five-second averages.

first arbitrarily applying a modification to the ISAF measurements employing an orthogonal distance regression (ODR) of the 10-s merged data. In this way a modified 1-s ISAF data set was generated using the ODR slope and intercept, and this was averaged with the CAMS data to arrive at a combined 1-s CH_2O data set (see Figure S4 in Supporting Information S1 in Cuchiara et al., 2020).

The high temporal resolution peroxides were measured on the DC-8 with the time-of-flight (ToF-CIMS) mass filter and tandem quadrupole mass filter (T-CIMS) chemical ionization mass spectrometers (T-CIMS) utilizing reaction with CF_3O^- (Amelynck et al., 2000; Crounse et al., 2006; Huey et al., 1996; St. Clair et al., 2010). Ambient CH_3OOH data are provided as the fraction of an isotopically labeled standard addition. The CH_3OOH to internal standard ratios were employed in determining CH_3OOH SEs like the mixing ratios for other species (Cuchiara et al., 2020). Here, we assume that the ratio between ambient CH_3OOH and its internal standard is constant throughout different sampled air masses, and breakdown of this assumption represents one of two potential sources contributing to the large variance in deduced CH_3OOH SE results.

Two passive trace gases, CO and CO_2 were chosen to quantify tracer transport and entrainment. The Atmospheric Vertical Observation of CO_2 in the Earth's Troposphere (AVOCET; Vay et al., 2011) instrument and the Differential Absorption CO Measurement instrument (DACOM; Sachse et al., 1987) measured CO_2 and CO, respectively.

In this study outflow regions of the storm clouds were initially identified by the IWC (2DS probes) and vertical winds and further refined to reflect regions of constant depressed H_2O_2 and constant elevated CH_2O and CH_3OOH, as illustrated by the shaded regions of Figure 2. These periods were further verified with aid of the DC-8 forward camera (Figure S2 in Supporting Information S1) and the examination of NEXRAD radar

images (Homeyer & Bowman, 2017) of maximum column reflectivity with aircraft wind vectors (Figures 1b and 1c) to confirm the airplane interception of a convective cloud. In some cases, as in Figure 2b and verified by forward camera videos, sub-segments of convective cloud intercepts were identified with clear air segments interspersed. Each sub-segment was treated independently and designated by different letters in Table S2 in Supporting Information S1.

The DC-8 intercepted three distinct cloud cores in two different environments, both of which are influenced by the same airflow (see airflow vector in Figure 1a). A total of 17 cloud intercepts (5 marine and 12 land) and two PBL samples were identified for analysis. Table S2 in Supporting Information S1 lists the intercept numbers, cloud core identifications, the beginning and end times and the average altitude (MMS GPS) for each cloud intercept.

For each outflow flight segment, entrainment and scavenging calculations used the average trace gas mixing ratios in the outflow over each segment, which contrasts with Cuchiara et al. (2020) who used peak values in the outflow segments because the peak values in CH_2O or minimum values for H_2O_2 were readily apparent in the 2 September storm cases, were very sharp, and were representative of the outflow averages. The 18 September marine and land intercepts exhibited significantly smaller enhancements or depressions (factors of ∼2–4 in the case of CH_2O) and displayed a wider spread over time with no clear sharp peak or depression (H_2O_2).

The model simulations were configured to estimate the transport and entrainment of soluble trace gases in convection, investigate the relationship between precipitation production and wet scavenging tendency, and analyze various processes that affect scavenging of CH_2O, H_2O_2, and CH_3OOH. The Weather Research and Forecast (WRF) model (Skamarock et al., 2008) version 3.9.1 was used to simulate the meteorological (meteorology and inert tracers) and chemical (WRF-Chem, Grell et al., 2005) conditions of the September 18th case. For the sake of consistency with previous SEAC^{4}RS simulations, much of the model configuration follows that of Cuchiara et al. (2020). The Supporting Information S1 provides more details of the configurations for the WRF-Chem simulations, including Table S2 in Supporting Information S1 summarizing the main model configuration and Figure S4 in Supporting Information S1 showing the location of the nested domains.

2.3. Analysis Methods

There are distinct approaches in the literature using observational and/or modeling analysis to determine SEs of trace gases in convective storms. These approaches range in complexity from a simple method that compares the ratio of a soluble to an insoluble (very slow reacting) trace gas that accounts for entrainment at inflow and outflow altitudes (e.g., Apel et al., 2012; Fried et al., 2016) to a more complex direct approach that compares the flux of soluble trace gases in rain at the surface to the flux of that trace gas entering the storm (e.g., Barth, Kim, Skamarock, et al., 2007; Easter & Hales, 1983). Note that this paper defines inflow as the region a few meters above the surface to cloud base. The identification of the intercept outflow regions was previously discussed in Section 2.2 and Table S2 in Supporting Information S1.

The analysis approach employed here is a multicomponent mixing model that follows the work of Barth et al. (2016), Cuchiara et al. (2020), and Fried et al. (2016), details for which are presented in the Supporting Information S1. Briefly, the multicomponent mixing model begins with the estimation of the dilution of trace gases due to the lateral entrainment rate (α) of background air into the cloud during convective transport. Two methods are used to estimate α: (a) using observed non-soluble trace gases, which we define as the Constant Column Entrainment method (CCE); and (b) using a WRF-simulated inert tracer to define different α values for each 1-km altitude, which we designate as the Variable WRF-Tracer Entrainment (VWE) method. The storm outflow soluble trace gas mixing ratio is then calculated using both α and clear air profiles, that is, regions near the storm where the DC-8 aircraft was sampling in cloud-free air. The difference between calculated (modified by entrainment) and measured mixing ratios is used to define the SEs for CH_2O, H_2O_2, and CH_3OOH. Table S3 in Supporting Information S1 presents the SE results employing both methods and the Text S2 in Supporting Information S1 provides further details for these calculations.

Wet scavenging in the WRF-Chem simulations employs the Neu and Prather (2012) scheme. The scavenging amount calculated for a given species depends upon the net precipitation production rate (precip. kg kg^{-1} s^{-1}) of rain, snow, and graupel from cloud water and ice minus evaporation at each model level during a time step. In the Neu and Prather (2012) scheme, the retention factor *rf* is applied to CH_2O, H_2O_2, CH_3OOH, and HNO_3 for

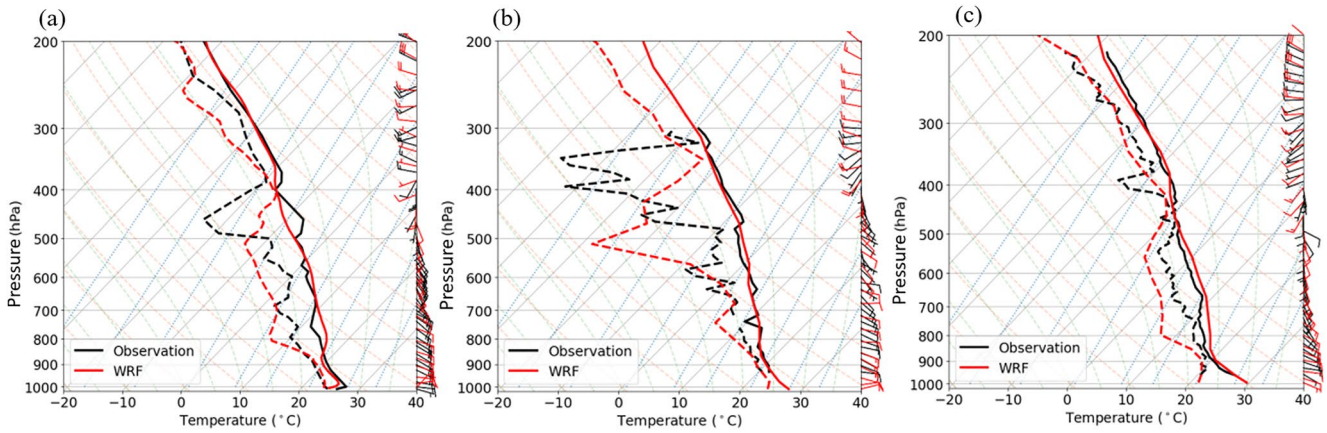

Figure 3. The Skew-T profiles (black) from (a) National Weather Service Corpus Christi, TX (CRP—27.76°S; −97.50°W) radiosonde at 12 UTC (b) DC-8 sampling region over marine convection (27.5°S; −96.5°W) at 16 UTC, and (c) DC-8 sampling over land convection (28.5°S; −99.0°W) at 17 UTC. The locations of these soundings are marked in Figure 1 as the open circle, cyan box, and gray box, respectively. The Weather Research and Forecast simulated results at 12, 16, and 17 UTC, respectively, are depicted in red. Solid lines represent temperature, and dashed lines represent dew point temperature. Along the right side are wind barbs (knots).

the temperature range of 0° to −15°C to account for retention of these trace gases during cloud drop freezing into snow and graupel. The standard *rf* values for CH_2O, H_2O_2, CH_3OOH, and HNO_3 are 0.64, 0.64, 0.02, and 1.0, respectively. All other trace gases have *rf* set to 0 at temperatures between 0° and −15°C. By differencing the simulations with and without the wet scavenging scheme the SE is determined as follows:

$$SE_{(\%)} = 100 \times \left(\frac{q_{i,noscav} + q_{i,scav}}{q_{i,noscav}} \right), \quad (1)$$

where $q_{i,noscav}$ and $q_{i,scav}$ are the mean outflow mixing ratios of species *i* in the simulation without wet scavenging and a simulation with wet scavenging turned on, respectively. The WRF-Chem SEs using different prescribed *rf* values are compared to the SE determined using the first two methods using observations. A polynomial fit is applied to the WRF-Chem simulation SE results to determine what fraction of the scavenged soluble species is retained in ice particles when cloud drops freeze. This approach, which was first presented in Cuchiara et al., 2020, allows us to investigate the trace gas partitioning between gas and condensed phases in the presence of cloud ice as detailed in Section 3.4.

3. Results

3.1. Model Performance Evaluation of Meteorology

Convective storms are complex systems that depend on many small-scale processes in the atmosphere. The challenges in representing these small-scale processes in numerical weather systems limits models from predicting the timing and the location of the convection accurately, consequently preventing the direct comparison between simulated and observed clouds. For this reason, we evaluate the meteorological performance of WRF on the representation of the thermodynamic structure of the atmosphere using radiosondes, DC-8 vertical profiles, and radar reflectivity. In general, there is good agreement between WRF-predicted and observed temperature, dewpoint temperature, and winds measured by the Corpus Christi, TX radiosonde and DC-8 vertical profiles (Figure 3).

The model simulates the temperature vertical profiles well at all levels except for the 450 hPa in the CRP profile (Figure 3a), where modeled values at approximately 450 hPa are lower than the observation at the same level. This level coincides with a dry layer that the model was not able to represent, and the dewpoint temperatures show a consistent wet bias at this level. While the sounding suggests that WRF-predicted convection could reach higher altitudes, the vertical profiles near the convection do not exhibit the mid-tropospheric inversion seen at Corpus Christi. Over the Gulf of Mexico (Figure 3b), the model captures a dry layer at 500 hPa which is below the observed dry layer at 350 hPa. The radiosonde over land (Figure 3c) presents a dry layer from 850 to 650 hPa that was overestimated by the WRF model. Overall, the wind speed and direction simulated by the model agree

with observations. The model captured most of the wind intensities and the wind shear at the level of approximately 400 hPa.

The WRF-Chem model replicates the observed marine-land surface air temperature field (Figure S5 in Supporting Information S1) and successfully reproduces the increase of air temperatures observed in surface stations during the day. Likewise, the surface winds match surface station observations fairly well. The PBL structure and height (Figure S5 in Supporting Information S1) near the convective storms were well simulated when compared to DC-8 PBL measurements for both the marine (PBL height ∼300 m) and land convection (∼1,500 m). Contour Frequency by Altitude Diagrams (CFADs) were evaluated to allow the calculation of the frequency distribution of radar reflectivity (Figure S6 in Supporting Information S1) as a function of height in moderate (Figure S7 in Supporting Information S1; precipitation rate of ∼0.2–2.5 mm hr^{-1}) and heavy precipitation (Figure S8 in Supporting Information S1; precipitation rate greater than 12 mm hr^{-1}). The frequency distribution of simulated moderate rainfall columns is well simulated for the Morrison et al. (2009, MORR) scheme, suggesting that WRF simulated the convective clouds relatively well, presenting similar microphysical properties for these two precipitation regimes. The WRF simulated reflectivity for the MORR microphysics scheme was compared with other schemes and outperformed the Thompson et al. (1994, THOM) and the WRF Single Moment 6-class (WSM6; Hong & Lim, 2006) cloud physics schemes. Thus, the main analysis of entrainment rates and SE are conducted with the MORR cloud physics scheme, while SE results from the other cloud physics schemes are discussed in Section 3.4.

3.2. Chemistry Simulation Performance Evaluation

Clear air profiles of key chemical constituents (CH_2O, H_2O_2, and CO) are compared between WRF-Chem results and DC-8 measurements to evaluate the prediction of the atmospheric composition. A comparison of CH_3OOH is not presented because of the lack of observed absolute mixing ratios for this compound (Section 2.2). The clear air profiles were evaluated for the two different regions of the DC-8 sampling periods due to expected differences in background chemistry between the marine and land areas. Thus, measurements from 15:30 to 17:00 UTC for the marine convection and 17:30–20:00 UTC for the land convection are binned by altitudes and averaged. The clear air criteria are based on total LWC and O_3–CO ratios (see Text S2 in Supporting Information S1). The vertical profiles include all the outflow and boundary layer flight legs over the full altitude range sampled, from approximately 0.5–10 km for the marine region and to 12 km above ground for the land region.

While modeled CH_2O profiles match observations well below 2 km (i.e., within the boundary layer) and above 8 km altitude, the WRF-Chem model underestimates the observations in the mid troposphere for the quasi-marine profile (Figure 4a). For the land region, WRF-Chem simulated CH_2O matches the observed vertical profile well (Figure 4e). Observations of H_2O_2 in the quasi-marine clear air show that WRF-Chem underestimated mixing ratios by up to 500 pptv below 2 km altitude and up to 200 pptv at 10 km altitude. In contrast, the land clear air profiles of H_2O_2 show good agreement below 2 km and above 10 km altitude but overestimate the H_2O_2 mixing ratios in the mid troposphere. The simulated CO matches with the observation above 6 km but WRF-Chem underpredicts observations by up to 20 ppbv below this level. The underestimation is consistent between marine and land atmosphere, suggesting a misrepresentation of an emission source. It is important to note the lack of vertical gradients of CO over both marine and land environments. This feature resulted in challenges in determining entrainment rates using the column method and required us to rely solely on CO_2 profiles (Figures 4d and 4h) instead. Note that the WRF-Chem does not simulate CO_2 with the configuration used in this work, so the CO_2 comparison is not presented in this comparison.

3.3. Derivation of Scavenging Efficiencies

During a cloud's lifetime, there is an important interaction between the large-scale environment and the cloud core via the entrainment of air into convective updrafts. As seen in Figure 4, the observed CO lacked a vertical gradient and therefore CO_2 was used to estimate entrainment rates for the land convection. However, the marine vertical gradients for both CO and CO_2 are negligible, rendering these two tracers unsuitable for determining entrainment with the CCE method. As a result, our marine convection cases exclusively rely on the WRF-tracers in the determination of entrainment rates. The average entrainment rate per kilometer (% km^{-1}) employing the VWE is $\alpha = 9.6 \pm 3.2\%$ km^{-1} ($N = 5$) for the marine intercepts. The land α value based on the CCE method yields

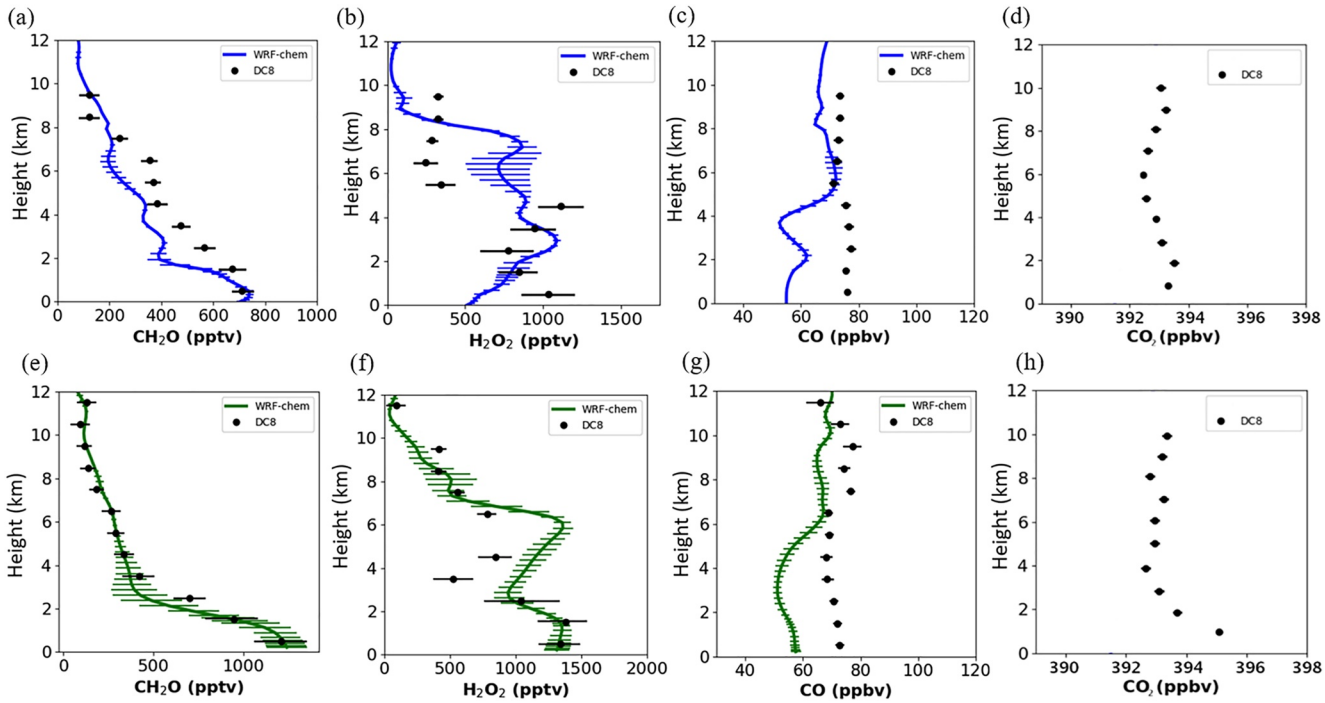

Figure 4. Clear air vertical mixing ratio profiles along the DC-8 flight track of (upper panels) marine and (bottom panels) land convection. Vertical profiles comparison between observed aboard the DC-8 (mean and standard deviation) and modeled (mean and standard deviation) (a and e) CH_2O (b and f) H_2O_2 (c and g) CO, and (d and h) CO_2 from 15:30 to17:00 UTC for the marine convection and the period between 17:30 and 20:00 UTC for the land convection along the DC-8 flight track.

$\alpha = 7.8 \pm 5.2\%$ km^{-1} ($N = 6$) and $\alpha = 10.4 \pm 5.4\%$ km^{-1} ($N = 6$) for cores 2 and 3, respectively. These land-based results are in reasonable agreement with the corresponding VWE determinations of $\alpha = 9.3 \pm 1.1\%$ km^{-1} and $8.7 \pm 0.4\%$ km^{-1}. Table S4 in Supporting Information S1 provides the entrainment rates for each 1-km altitude layer based on the VWE method.

Figure 5 provides a summary of SEs using the average of the CCE and VWE methods for case studies derived from the September 18th case alongside SEs determined for land convection on September 2nd during SEAC^{4}RS and a variety of land convection cases (6 case studies) during the DC3 field experiment. The error bars on each result represent the standard deviation of the SE determinations from the two entrainment methods. The number of estimated SEs (labeled in each panel) is the product of the number of intercepts for each storm and the two entrainment methods. The average CH_2O SE for the 18 September intercept over the Gulf of Mexico (blue triangle) at a 2.5 km altitude yields a SE of $16 \pm 4\%$ ($N = 2$, average of two ER methods), which agrees with the low altitude September 2nd SE ($6 \pm 9\%$) value over land. Note that at these low altitude levels, most of the precipitation production happens in the liquid-only warm regions of the cloud and the cloud physics-trace gas interactions follow Henry's Law. The low altitude CH_2O SEs agree with those predicted by Henry's Law equilibrium calculations (Text S3 in Supporting Information S1). At mid to high altitudes (6–12 km), the CH_2O SEs do not show differences outside one standard deviation of their average between the marine and land convection, with composite averaged SE of $44 \pm 7\%$ ($N = 8$) and $53 \pm 10\%$ ($N = 24$), respectively. The mid to high altitudes (6–12 km) CH_2O SE results for the September 18th storms (land and marine) overlap with the September 2nd land case and these in turn overlap, within the uncertainty limits, with the DC3 values of SE = $52 \pm 7\%$ for more severe convection (composite average of 29 May, 6 June, 11 June, and 22 June results, Fried et al., 2016). Table S3 in Supporting Information S1 lists the SEs for the individual intercepts.

The H_2O_2 SEs (Figure 5b) reveal high values ranging between 80% and 90% in both the marine and land convection on 18 September in the 6–12 km altitude range and do not show differences outside one standard deviation of their average between the marine and land convection (the marine SE = $85 \pm 6\%$, $N = 6$, and land SE = $90 \pm 5\%$, $N = 20$). These high SEs for H_2O_2 are expected due to its high solubility. At lower altitudes, the H_2O_2 SEs are ~35% for September 2nd land convection and 83% for the marine convection on 18 September, where the latter SE is in line with Henry's Law equilibrium calculations (Text S3 in Supporting Information S1). The former

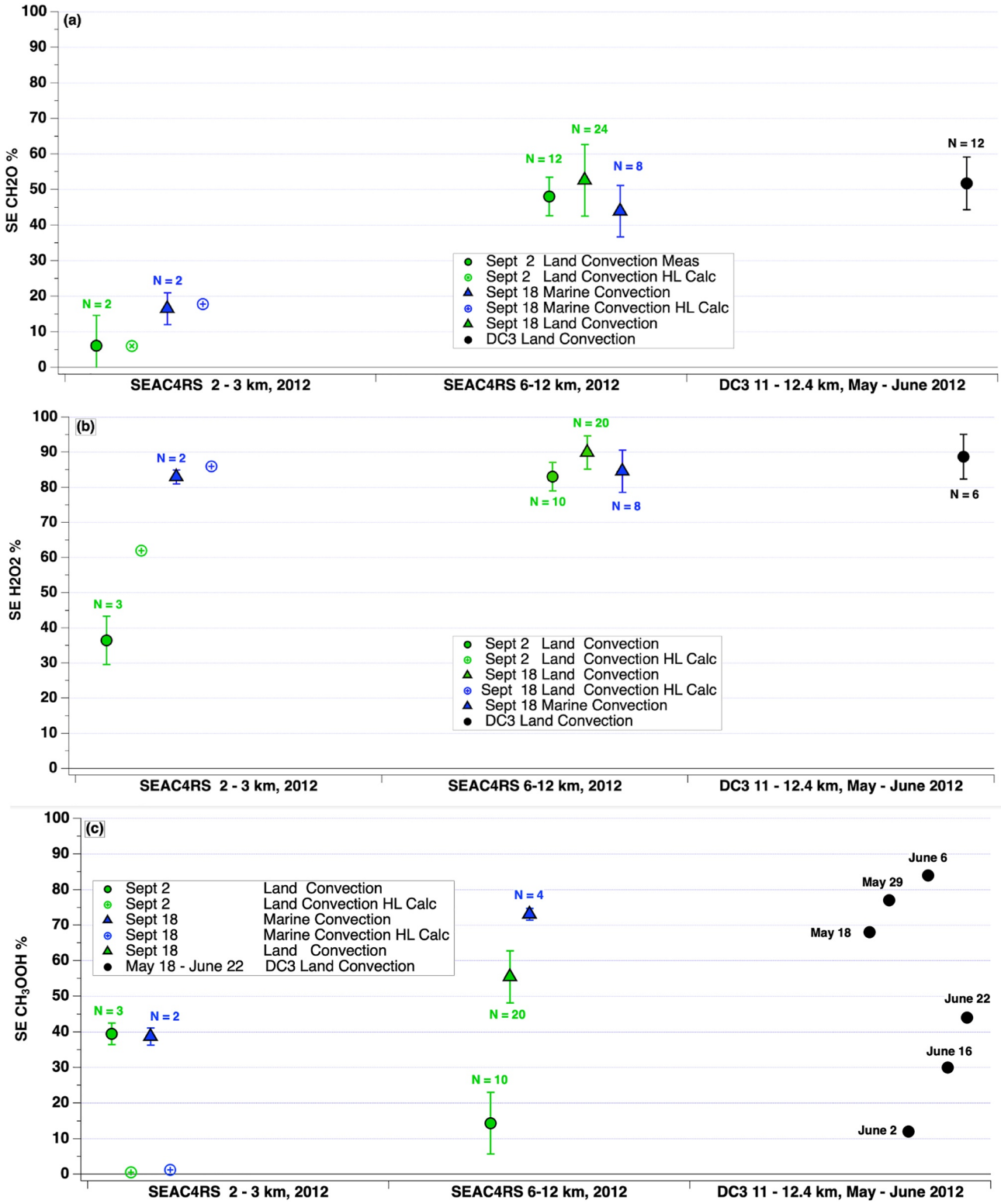

Figure 5. The average and standard deviation of CH_2O (a), H_2O_2 (b), and CH_3OOH (c) scavenging efficiencies (SEs) for intercepts at altitudes between 2–3 and 6–12 km in the SEAC^{4}RS campaign, and at altitudes between 11 and 12.4 km in the DC3 campaign. Blue and green triangles represent marine and land convection, respectively, on 18 September 2013. Black points show results from storm intercepts during the DC3 campaign (Barth et al., 2016). The open circles with crosses are the calculated SEs assuming Henry's Law (HL) equilibrium.

value, however, is considerably lower than the Henry's Law equilibrium value, possibly due to differences in LWC but we have no explanation for this difference for now.

The CH_3OOH SE values (Figure 5c) in DC3 and SEAC^{4}RS (both 2 and 18 September cases) span a large range, which cannot be fully explained. The error bars for the SEAC^{4}RS cases represent the 1σ imprecisions of the average values for each measurement grouping. The error bars on the DC3 CH_3OOH SE results, which are not shown here due to their magnitudes, are based on uncertainties in the measurements (Table 9 of Barth et al., 2016). The six DC3 CH_3OOH SE estimates ranged from 12% to 83% with individual storm 1sigma error bars that averaged ±38%. The September 2nd convection at 6–12 km over land yields a CH_3OOH SE of 14 ± 9%, based upon an average of both entrainment methods (Cuchiara et al., 2020), which is in line with that expected due to the mild CH_3OOH solubility. However, the marine 18 September convection CH_3OOH SE of 39 ± 2% at low altitude (2–3 km), and the similar 2 September low altitude land convection CH_3OOH SE of 40 ± 3% as well as the high altitude 18 September marine SE of 73% ± 2% ($N = 4$) and land SE of 56% ± 7% ($N = 20$) are all considerably higher than expected for CH_3OOH (Text S3 in Supporting Information S1). Several DC3 storms also showed SEs greater than expected values. This will be further discussed in Section 4.

3.4. WRF-Chem Estimated Scavenging Efficiencies and Ice Retention Factors

By differencing two simulations, one with wet scavenging and one without wet scavenging operating, the WRF-Chem SE can be determined (see Section 2.4 for more detail on the methodology). Scavenging efficiencies were determined by employing three cloud physics schemes, the Morrison et al. (2009) double-moment scheme (MORR), the Thompson et al. (2008) scheme (THOM), and the WRF single-moment 6-class scheme (WSM6) from Hong and Lim (2006), assuming ice retention factors of 1, and analyzing the simulated clouds over 8 hr of simulation over land and over water. During this averaging period, the storms are at different stages of development (growing, mature, decaying) and the population of clouds changes using different cloud physics schemes (Figure S6 in Supporting Information S1). Consequently, the average LWC in the marine region is lower than that in the land region, opposite of what was found in the analysis of the single storms discussed earlier. The lower average LWC in marine region also means that the SEs are lower in the marine region compared to the land region (Figure S9 in Supporting Information S1). All three cloud physics schemes predict very low SEs (0%–5%) for CH_3OOH throughout the entire vertical profile. The MORR and WSM6 schemes predict higher CH_2O and H_2O_2 SEs than the THOM scheme. Also, THOM scheme is showing more ice and snow in the marine case, which is evidence of more cloud water being lofted into the mixed phase region. Differences in the SEs caused by the different cloud physics schemes can be attributed to their different vertical profiles of cloud water, rain, ice, snow, and graupel, which is a result of some of the assumptions made for various cloud processes, such as the type of precipitation formed from riming. The SE results from MORR and WSM6 schemes are more consistent with the observations, although there are still some major discrepancies with the observations.

The cloud hydrometeor spatial distribution and production of precipitation from cloud water play an important role in the scavenging of trace gases and the in-cloud gas-phase trace gas vertical profile. Using individual simulated cloud results from the WRF-Chem model employing the MORR scheme, the in-cloud (i.e., grid columns with QCLOUD > 10 μg kg^{-1}) gas-phase CH_2O, H_2O_2, and CH_3OOH vertical profiles show different rates of depletion with altitude (Figure 6). As found by Cuchiara et al. (2020), a considerable amount of CH_2O is transported through the warm phase of the cloud entering the mixed-phase regions (~5–7 km height, temperature range ~0°C– ~ −15°C indicated in the middle sections) making CH_2O susceptible to scavenging by snow and graupel through cloud drop freezing and, hence, the ice retention factor may come to play here. In contrast, the highly soluble H_2O_2 has very little gas phase H_2O_2 entering the mixed-phase regions of both marine and land storms (Figure 6b), with substantial depletion below the freezing level. Like CH_2O, in-cloud, gas-phase CH_3OOH (Figure 6c) shows a considerable amount of CH_3OOH entering the mixed-phase region. The in-cloud, gas-phase CH_3OOH mixing ratios are the same for both simulations with and without scavenging with only small differences occurring at temperatures colder than 264 K suggesting that cloud drop freezing between 264 and 273 K is a minor pathway for CH_3OOH scavenging. It is important to note that the simulations with the scavenging scheme turned on (dashed lines in Figure 6) were all carried out using an ice retention factor of 1 (i.e., no gas re-emission), which yields the maximum amount scavenged.

In addition, the WRF-Chem model SE results provide the ability to examine the role of ice retention in freezing drops by prescribing the ice retention factor (*rf*). Several WRF-Chem sensitivity simulations were conducted with

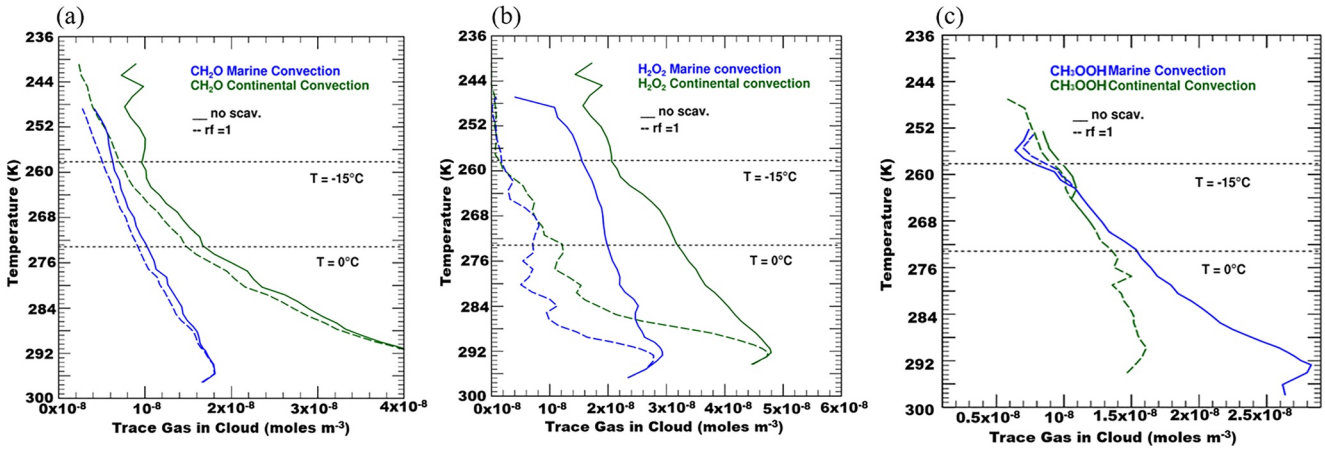

Figure 6. WRF-Chem simulated in-cloud gas-phase concentration with (dashed line) and without (solid line) scavenging scheme on for (a) CH_2O, (b) H_2O_2 and (c) CH_3OOH for the marine (blue) and land (green) convection. The results are from the simulation using the Morrison et al. (2009) cloud physics scheme.

different *rf* values to provide bounds around the observed SE. The *rf* value with an estimated range is then determined by matching the observed averaged values with those from an empirical 3-term polynomial fit of these simulations (Figure 7). In the case of CH_2O, the 18 September marine and land *rf* values fall within the range of 0.5–0.8, and 0.5 and 0.9, respectively. The corresponding H_2O_2 values fall in the range between 0.3 and 0.5 for the marine cases and between 0.3 and 0.4 for the land cases. In Section 4, we discuss the relationship between these values with those from other studies and in the process highlight persistent uncertainties requiring additional investigation. The WRF-Chem simulations predicted SE between 0%—5% for CH_3OOH regardless of what *rf* was prescribed. Therefore, we cannot make an estimate of what the retention factor is for CH_3OOH.

4. Discussion

The H_2O_2 *rf* range of 0.3–0.5 of the present study (average value ~0.4) deduced from Figure 7 agrees with both wind tunnel measurements ($rf = 0.52 \pm 0.08$; Jost et al., 2017) and our previous studies (0.1–0.4 range estimated for the 2 September storm cases; Cuchiara et al. (2020) and the $rf < 0.25$ simulated by Bela et al. (2018)). Thus, H_2O_2 presents a consistent story amongst the various storm types in terms of SE and *rf* values, most likely because H_2O_2 is scavenged in the liquid region of the storm (Figure 6). Likewise, the CH_2O SE determinations of the present September 18th land and marine convection cases are consistent with those measured during land DC3 and the 2 September storm cases, all of which yield values ~50%, yet contrast with previous studies (Borbon et al. (2013) who reported CH_2O SEs of 4%–39%, and Bozem et al. (2017) who reported CH_2O SEs of 0%–47%). However, we point out that the Bozem 0%–47% range is not the range deduced from independent measurements but represents the range of deduced CH2O SEs from the simulated temporal evolution of CH_2O in the outflow region estimated to be 20–50 min downwind of the core. The 0%–47% range thus reflects the range of deduced CH2O SEs by randomly varying rate constants and concentrations in their simulations. Furthermore, it is important to re-emphasize the findings of Fried et al. (2016) where errors in selecting the appropriate corresponding BL inflow region connected to the OF can result in low SE determinations. As discussed in that study, such errors can be particularly prevalent in cases with large BL isoprene levels.

Considering the DC3 and SEAC4RS case studies, two major unresolved questions have been raised, which we address in this section. The unresolved questions are: (a) the large unexplained range of CH_2O *rf* values determined in the DC3 studies and SEAC^{4}RS storm cases as well as additional CH_2O *rf* values from other studies; and (b) the large unexplained range (10%–85%), as well as high values for CH_3OOH SEs, measured during the SEAC^{4}RS and DC3 campaigns. The high SE values are quite surprising given the low solubility for CH_3OOH.

4.1. Discussion of CH_2O Ice Retention Factors

Our studies for the 2 September and 18 September SEAC^{4}RS storm cases compared with those from DC3 range from <0.25 to 0.9 for the determined CH_2O *rf* factor (Figure 8). In contrast, the modeling study of Leriche

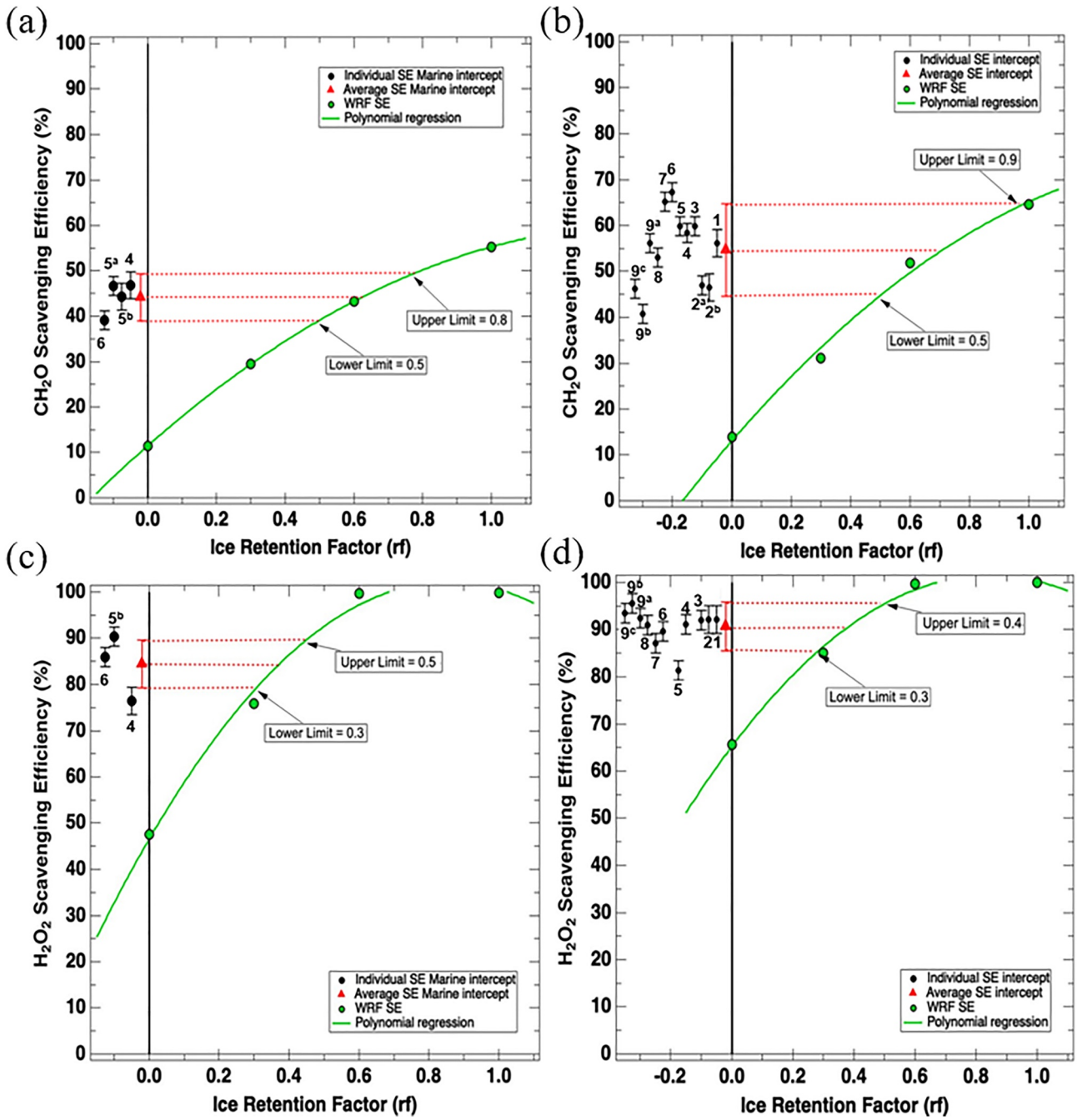

Figure 7. WRF-Chem scavenging efficiencies (SEs) (dots) for different *rf* of CH_2O (a and b) and H_2O_2 (c and d) of the selected simulated marine at 15:30 UTC (left column) and land at 18:50 UTC (right column) in-cloud outflow region averaged for total condensed water >0.01 g kg^{-1} and between 7 and 9 km altitude, and individual in-cloud SEs derived from observations (black points) and averaged values (red triangle). The lines are empirical 3-term polynomial fits.

et al. (2013) recommends a CH_2O rf value of 0.64, while the University of Mainz vertical wind tunnel studies (Jost et al., 2017) report a CH_2O rf value of 0.97 ± 0.11, explaining that the high CH_2O *rf* was because CH_2O (aq) is hydrolyzed to methanediol, which needs to dehydrate before CH_2O can be released to the gas phase. The wind tunnel studies represent dry growth riming where supercooled liquid droplets containing CH_2O were collected by ice and snow hydrometeors falling at their terminal fall velocities from 2 to 3 m s^{-1} and subsequently freezing. Hence, these experiments occurred in less turbulent conditions than convective storms. One single CH_2O *rf* value cannot describe this parameter under all conditions; as a result, this produces uncertainty when modeling UT HO_x and O_3 chemistry in convective outflow regions due to CH_2O convective transport using a single CH_2O *rf* value or

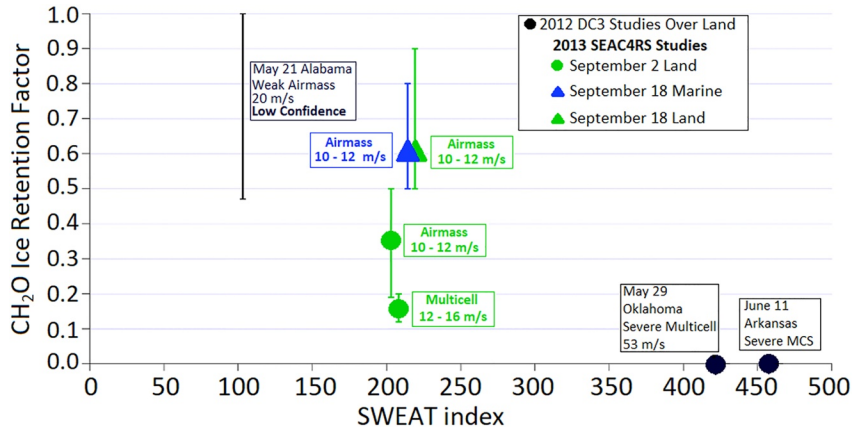

Figure 8. CH_2O ice retention factors and Severe Weather Threat (SWEAT) index for the various storm cases studied during the DC3 campaign (black), and the 2 and 18 September 2013 SEAC^{4}RS studies (green—studies over land and blue—studies over water). The points indicate the average value while the lines indicate the range of retention factors determined during the SEAC^{4}RS studies. The annotation by each case identifies the storm type and maximum vertical velocity estimate. For both SEAC^{4}RS cases, the SWEAT values were offset by 5 SWEAT units to show both storms sampled on each of the 2 days.

a simple parameterization. In the discussion that follows, we present one hypothesis that might explain the wide range of reported CH_2O *rf* values, namely: the presence of strong dynamic forces in severe convection, which we speculate can mechanically shatter various forms of ice hydrometeors, releasing trapped gas and liquid-phase CH_2O back into the gas phase. Two parameters that can be used to characterize substantially turbulent convection are maximum vertical velocity and the Severe Weather Threat (SWEAT) Index. This index is determined from several variables involving differences in wind speed, wind direction, and temperatures at two different altitudes (850 and 500 mb) to determine the likeliness of severe weather and tornadoes. Operationally SWEAT values between 150 and 300, between 300 and 400, and above 400 indicate the potential for slightly severe, severe, and tornadic storms, respectively. We hypothesize that mechanical ice shattering using the low vertical velocities employed in the wind tunnel studies is less important, if at all, compared to our in-storm convective studies.

Figure 8 summarizes the CH_2O *rf* values determined from three DC3 storms over land as well as the 2 September 2013 land and 18 September SEAC^{4}RS land and marine storms as a function of the SWEAT index. The estimated maximum vertical velocities (measured from the onboard APR2 radar images in the case of SEAC^{4}RS) are given next to each determination. The markers reflect the best *rf* determinations, values for which during the DC3 storms are published by Bela et al. (2016, 2018). Cuchiara et al. (2020), and Fried et al. (2016) published *rf* CH_2O values for two different 2 September SEAC^{4}RS storms over land, an airmass storm, and a multicellular storm. These two storms have identical SWEAT values (offset by 5 SWEAT units for clarity) and similar averaged maximum vertical velocities in the 10–16 m s^{-1} range. The 18 September *rf* CH_2O values over land and marine environments of the present study are likewise offset by 5 units and have similarly low averaged maximum vertical velocities in the 10–12 m s^{-1} range.

The 2 and 18 September SEAC^{4}RS cases employed multiple storm intercepts to arrive at averaged *rf* values with uncertainty limits, which are not symmetric about the average (Figure 7). These limits reflect the large range of *rf* values employed in the WRF-Chem cloud simulations that match the averaged SE observations with their associated standard deviations employing a 3-term polynomial fit. These limits are indicated in Figure 8 by horizontal symbols at both ends of the *rf* range. By contrast, limited storm intercepts in the DC3 studies were employed, with two intercepts in the 29 May case and one each for the other two cases. Also, the WRF-Chem sensitivity simulations for the DC3 cases were conducted for a limited number of *rf* values, which prevents us from placing similar precision bounds on the *rf* values for the three DC3 storms.

However, for the two severe DC3 storm cases (29 May and 11 June), the WRF-Chem cloud simulations match the SE determinations at *rf* values around 0. The 21 May weak airmass case during DC3 yields a *rf* value $=0.7 \pm 0.25$ based on the values in Figure 7 of Bela et al. (2018). However, Fried et al. (2016) show that the CH_2O SE determinations for this intercept are highly uncertain since the inflow and outflow i/n-pentane ratios are significantly different, which reflects airmasses of different origins and ages. For these reasons, we indicate Low Confidence for the 21 May DC3 determination.

The 29 May DC3 storm exhibited the highest maximum vertical wind velocity with values averaging 53 m s^{-1} (DiGangi et al., 2016) and a SWEAT index >400; the 29 May DC3 storm produced a tornado and fist-sized hail. The severe MCS11 June case also had a SWEAT index >400. Although no NEXRAD analysis of vertical wind speeds is available for the MCS 11 June case, Giangrande et al. (2013) report maximum vertical velocities >20 m s^{-1} for MCS cases over Oklahoma. Both cases resulted in CH_2O *rf* values around 0, which is consistent with our speculation that *rf* is smaller in strong convection when ice shattering can occur. Likewise, the three SEAC^{4}RS airmass storm cases with lower vertical velocities in the 10–12 m s^{-1} range and lower SWEAT values (~200) yield averaged *rf* values in the 0.35–0.6 range, with limits extending from 0.19 to 0.9, which again is consistent with our hypothesis. The slightly higher maximum vertical velocities for the multicellular September 2nd SEAC^{4}RS storm case (12–16 m s^{-1} range) over land, yields a *rf* value of 0.16 ± 0.04 at a SWEAT value of 203. Collectively, the analysis suggests higher CH_2O *rf* values (range 0.12–0.9) at lower SWEAT indices and lower maximum vertical velocities than the two DC3 cases.

As can be seen in Figure 7, the ice retention determinations are not only dependent upon the scatter in the observed CH_2O SE estimations but are also particularly sensitive to the precise shape of the WRF-Chem SE-ice retention profiles. As discussed in Cuchiara et al. (2020), the shape of these profiles in turn are very sensitive to the precise convective core selected in the simulations to match the observed convection. Even using a high-resolution ($\Delta x = 1.35$ km) WRF-Chem simulation in the 2 September cases, we still encounter uncertainties in the simulations due to the natural small, subgrid-scale characteristics of the observed clouds, and this represents a potential weakness in our method of determining ice retention factors. Compare, for example, the two SE-ice retention profiles shown in Figure 9 of Cuchiara et al. (2020) for the September 2nd airmass and multi-cellular storms, which we reproduce in Figure S10 in Supporting Information S1. Despite similar observed CH_2O SEs around 50%, the shape of the two SE-ice retention profiles is significantly different, which in turn results in two different *rf* values.

Although our speculation regarding mechanical shattering of various forms of ice hydrometeors is a reasonable hypothesis to explain the large range of CH_2O *rf* values, more studies are needed before definitive conclusions can be drawn. In particular, future efforts need to focus on additional case studies with an emphasis on more detailed and finer resolution subgrid-scale WRF-Chem cloud modeling.

4.2. Discussion of the Large Range for CH_3OOH SEs

Based on Henry's Law calculations, CH_3OOH SEs should be small (<10%). The high CH_3OOH SEs estimated in this study and by Barth et al. (2016) are surprising compared to this expected SE value. As noted by Allen et al. (2022) and Cuchiara et al. (2020), laboratory measurements of CH_3OOH using the Caltech CIMS instrument revealed an isobaric interference due to methanediol ($CH_2(OH)_2$, hydrated CH_2O), which is detected efficiently by the Caltech CIMS instrument in high water vapor regions, such as the boundary layer. Franco et al. (2021) discuss the mechanism by which gaseous CH_2O dissolved in cloud water rapidly hydrates to form $CH_2(OH)_2$ in solution, which under typical warm cloud conditions (275–290 K) degasses to produce $CH_2(OH)_2$ directly in the gas phase. The gas phase $CH_2(OH)_2$ that does not go on to react with OH in producing formic acid, could thus represent an interference in the measured CH_3OOH that behaves differently in the lower atmosphere relative to the higher altitude outflow. Allen et al. (2022) estimated the potential interference of $CH_2(OH)_2$ on the Caltech CIMS CH_3OOH measurement in relation to the water vapor measurements taken during the ATom field campaign using measured CH_2O and estimated Henry's Law constant for $CH_2(OH)_2$. Because the Henry's Law constant for $CH_2(OH)_2$ has not been published, Allen et al. (2022) estimated its value based on analog compounds like hydroxy methylhydrogen peroxide and ethanediol, finding Henry's Law constant on the order of 2×10^6 M atm^{-1} for the measured ATom conditions that it is similar to what Müller et al. (2021) derived but higher than that estimated by Franco et al. (2021) of $0.1–10 \times 10^5$ M atm^{-1}. Allen et al. (2022) found a 5% or less fractional contribution of $CH_2(OH)_2$ to the CH_3OOH measurement for water vapor mixing ratios below 4,000 ppmv for both their best estimate $CH_2(OH)_2$ Henry's Law constant and a Henry's Law constant 10 times smaller. Thus, $CH_2(OH)_2$ interference on the CH_3OOH measurements is negligible for the convective outflow samples examined in the 18 September storms for altitudes above 8 km where water vapor mixing ratios were <3,500 ppmv. At water vapor mixing ratios typical for the boundary layer (12,000–30,000 ppmv), the results of Allen et al. (2022) indicate a 5%–12% and 12%–50% fractional contribution due to $CH_2(OH)_2$ on the CH_3OOH measurement for the best estimate $CH_2(OH)_2$ Henry's Law constant and a Henry's Law constant 10 times smaller, respectively.

Using water vapor measurements in the SEAC^{4}RS 18 September storm inflow regions, we estimate that the fractional contribution of $CH_2(OH)_2$ interference on the CH_3OOH measurements is 7% and 42% for the best estimate $CH_2(OH)_2$ Henry's Law constant and a Henry's Law constant 10 times smaller, respectively. Adjusting the CH_3OOH inflow measurement by this fraction, we find that the calculated CH_3OOH SEs are reduced from 56% to 54% (2% change) and from 56% to 40% (16% change) using the best estimate $CH_2(OH)_2$ Henry's Law constant and a Henry's Law constant 10 times smaller, respectively, for the land convection. For the marine convection, the calculated CH_3OOH SEs are reduced from 73% to 72% (1% change) and from 73% to 63% (10% change) using the best estimate $CH_2(OH)_2$ Henry's Law constant and a Henry's Law constant 10 times smaller, respectively. Note, that the adjusted CH_3OOH SE using the lower $CH_2(OH)_2$ Henry's Law constant is still greater than expected for the mildly soluble compound, which is <10% based on Henry's Law equilibrium. Thus, the $CH_2(OH)_2$ interference on the CH_3OOH measurements cannot fully explain the higher-than-expected CH_3OOH SEs that are determined here. For the DC3 cases, the Colorado storms analyzed had water vapor of <14,000 ppmv in the inflow regions, which likely will not cause an appreciable effect on the estimated CH_3OOH SEs. The Oklahoma storms had higher water vapor mixing ratios (22,000–24,000 ppmv) and therefore the $CH_2(OH)_2$ interference could cause the CH_3OOH SEs to decrease from 77% to 75% (for the best estimate of $CH_2(OH)_2$ Henry's Law constant) or to 62% (for a $CH_2(OH)_2$ Henry's Law constant 10 times smaller) for the May 29th Oklahoma storm and from 30% to 28% (for the best estimate of $CH_2(OH)_2$ Henry's Law constant) or to 11% (for a $CH_2(OH)_2$ Henry's Law constant 10 times smaller) for the June 16th Oklahoma storm. Except for the June 16th storm with lower $CH_2(OH)_2$ Henry's Law constant, the CH_3OOH SEs calculated for the DC3 storms remain higher than expected when the interference by $CH_2(OH)_2$ is accounted for.

5. Conclusions

In this study, observation techniques are combined with modeling analysis to investigate wet scavenging processes impacting trace gases in convective storms using a case study that occurred on 18 September 2013 during the SEAC^{4}RS campaign. Both the convection over the Gulf of Mexico and near San Antonio, Texas, which occurred in the same southeasterly onshore wind flow, were sampled and analyzed. The DC8 aircraft in situ measurements confirmed higher CCN, cloud base height, and higher vertical velocities for the land convection compared to the marine convection. Thus, we examined whether differences in storm morphology cause differences in convective transport and scavenging of the soluble trace gases CH_2O, H_2O_2, and CH_3OOH. These gas-phase species when transported to higher altitudes of the atmosphere become important precursors for HO_x radicals and therefore tropospheric O_3. The O_3 and HO_x production will vary in a complex nonlinear behavior depending on the NO_x and VOC abundance transported to the anvil from the boundary layer and the amount of NO_x produced by lightning. Recent studies (e.g., Apel et al., 2012, 2015; Hudman et al., 2007; Pickering et al., 1992) have estimated that 4–15 ppbv of O_3 will be produced per day due to high NO_x and enhanced concentrations of HO_x precursor species in the upper troposphere. Individual processes impacting wet scavenging such as the lateral entrainment of background air into the convective core and ice retention factors (*rf*) were also estimated.

The calculated SE averages for CH_2O (44%–53%, marine and land, respectively) and H_2O_2 (85%–90%, marine and land, respectively) from 6 to 12 km altitude range do not show differences outside one standard deviation of their average between the marine and land convection. For H_2O_2, the scavenging in the liquid-only region of the storms dominate its loss process, as aqueous-phase chemistry is likely not substantive with SO_2 mixing ratios below 100 pptv in both the marine and land environments sampled. Bela et al. (2018) found that the contribution of scavenging and entrainment affected the SE results more than that by chemistry. These results are in agreement with the more severe DC3 convective cases (Barth et al., 2016; Bela et al., 2016; Fried et al., 2016), and the airmass and multicell storms presented by Cuchiara et al. (2020) where highly soluble trace gases tend to be completely scavenged in the warm region of the cloud, that is, below 0°C isotherm.

For CH_2O, the similar SEs between marine and land convection are likely a result of the interplay of scavenging and storm dynamics (entrainment and turbulence) as CH_2O was shown to be transported into the mixed phase region (0°C to −15°C) of the storm where it is affected by ice-water physics processes. The present study determined ice retention factors (*rf*) values of CH_2O in precipitating ice during freezing processes. For the moderately soluble gas CH_2O, a range of *rf* values from near 0 to 1 are found based on this and previous studies. For the 18 September land and marine convection cases, we determined a *rf* range spanning values from 0.5 to 0.9, which is higher than the range determined by Cuchiara et al. (2020) for storms studied on 2 September 2013 (0.12–0.2

multicell; and 0.19–0.5 airmass), and significantly higher than values near 0 for two severe DC3 storm cases. Based on the relationship between *rf* and SWEAT index as well as vertical wind velocities, we hypothesize that ice shattering may play an important role in governing CH_2O *rf* values. Under this hypothesis, in severe convection, ice shattering may release trapped ice-bound CH_2O back into the gas phase. This is clearly an area where more studies are needed before definitive conclusions can be drawn. Measurements employing a storm penetrating aircraft would be especially valuable. In addition, modeling of small convective clouds, such as the marine convection, is better accomplished with higher grid resolution (250 m grid spacing or smaller) that will give more model grid points of both the convective cores and outflow regions. Despite the computational costs, combining high grid resolution and complex chemistry is important for advancing our understanding on the effects of convection on atmospheric composition.

A second area requiring attention in future studies relates to the highly variable and large CH_3OOH SEs determined during the SEAC^{4}RS and DC3 campaigns. This is quite surprising given the mild CH_3OOH solubility (Henry's Law constant at 298 K is 310 M atm^{-1}). For six DC3 storms studied, Barth et al. (2016) report CH_3OOH SEs of 20%–85%, with individual daily 1σ error bars that average ±38%. This contrasts with the September 2nd SEAC^{4}RS convection at 6–12 km over land, which yields a CH_3OOH SE of 14 ± 9%, based upon an average of two entrainment methods (Cuchiara et al., 2020), which is in line with the expected SEs for CH_3OOH. However, the corresponding SEs for the 18 September low altitude (2–3 km) marine convection (39 ± 2%) and a similar low altitude value for the 2 September land convection as well as the upper troposphere 18 September marine SE of 73% ± 2% ($N = 4$) and land SE of 56% ± 7% ($N = 20$) are all considerably higher than these expectations. Allen et al. (2022) noted the Caltech CIMS instrument, used to obtain CH_3OOH measurements in DC3 and SEAC^{4}RS, has an isobaric interference due to $CH_2(OH)_2$ (hydrated CH_2O) at high water vapor mixing ratios such as in the boundary layer. However, even after accounting for this interference and assuming 1×10^5 M atm^{-1} Henry's Law value for $CH_2(OH)_2$ (which is likely a factor of 10 low), the marine CH_3OOH SE drops only to 63% and the land CH_3OOH SE drops only to 40%. Thus, the $CH_2(OH)_2$ interference on the CH_3OOH measurements cannot fully explain the higher-than-expected CH_3OOH SEs that are determined here, a result that clearly warrants further investigation.

The present study raises two important questions requiring additional studies: the specific mechanism(s) responsible for the wide range of CH_2O ice retention values, and the unexpectedly large and variable values of the CH_3OOH SEs. Despite these issues, the present study also strengthens our understanding of CH_2O and H_2O_2 SEs under a broader set of conditions involving both marine and land convection where similar results were obtained and where results agree with previous studies during both SEAC^{4}RS and DC3.

Acknowledgments
We would like to thank NASA for supporting this research through grant NNX17AH52G, and specifically, Dr. Richard Eckman who oversees NASA's Aura Science Team and Atmospheric Composition Modeling and Analysis Program (ACMAP). NCAR is sponsored by the National Science Foundation. This work was supported in part by the NOAA Cooperative Agreement with CIRES, NA17OAR4320101 and NA22OAR4320151. We thank NASA for supporting the SEAC^{4}RS campaign, the NASA SEAC^{4}RS project leaders, and all the SEAC^{4}RS investigators for their data contributions. We thank Paul O. Wennberg, John D. Crounse, Jason M. St. Clair, Michelle Kim, Simone Tanelli, Glenn M. Wolfe, and Thomas F. Hanisco for collecting the aircraft measurements used in this study. We also thank Nicholas Heath for his support on CFADs scripts. We acknowledge the use of the WRF-Chem preprocessor tools (mozbc, fire_emiss, and bio_emiss) provided by the Atmospheric Chemistry Observations and Modeling Lab (ACOM) of NCAR and the supercomputer Cheyenne maintained by the Computational and Information Systems Laboratory (CISL) at NCAR.

Data Availability Statement

All data sets used in this paper are publicly available. All aircraft data were obtained from the NASA Langley Research Center Atmospheric Science Data Center (https://www-air.larc.nasa.gov/cgi-bin/ArcView/seac4rs; Chen, 2013, https://doi.org/10.5067/Aircraft/SEAC4RS/Aerosol-TraceGas-Cloud). The NOAA Next Generation Radar (NEXRAD) Level 2 Base Data is available at https://doi.org/10.7289/V5W9574V (NOAA National Weather Service Radar Operations Center, 1991). The National Weather Service radiosonde is available at https://weather.uwyo.edu/upperair/sounding.html. The WRF-Chem v.3.9.1.1 source code is available via https://doi.org/10.5065/D6MK6B4K. The model meteorological input data are available at https://rda.ucar.edu/datasets/ds608.0/ (National Centers for Environmental Prediction/National Weather Service/NOAA/U.S. Department of Commerce, 2005) and the CESM2.1/CAM-chem model input data at https://doi.org/10.5065/NMP7-EP60 (Buchholz et al., 2019).

References

Allen, H. M., Crounse, J. D., Kim, M. J., Teng, A. P., Ray, E. A., McKain, K., et al. (2022). H_2O_2 and CH_3OOH (MHP) in the remote atmosphere: 1. Global distribution and regional influences. *Journal of Geophysical Research: Atmospheres*, *127*(6), e2021JD035701. https://doi.org/10.1029/2021JD035701

Amelynck, C., Schoon, N., & Arijs, E. (2000). Gas phase reactions of CF3O− and CF3O−H2O with nitric, formic, and acetic acid. *International Journal of Mass Spectrometry*, *203*(1–3), 165–175. https://doi.org/10.1016/S1387-3806(00)00321-3

Apel, E. C., Hornbrook, R. S., Hills, A. J., Blake, N. J., Barth, M. C., Weinheimer, A., et al. (2015). Upper tropospheric ozone production from lightning NO_x-impacted convection: Smoke ingestion case study from the DC3 campaign. *Journal of Geophysical Research: Atmospheres*, *120*(6), 2505–2523. https://doi.org/10.1002/2014JD022121

Apel, E. C., Olson, J. R., Crawford, J. H., Hornbrook, R. S., Hills, A. J., Cantrell, C. A., et al. (2012). Impact of the deep convection of isoprene and other reactive trace species on radicals and ozone in the upper troposphere. *Atmospheric Chemistry and Physics*, *12*(2), 1135–1150. https://doi.org/10.5194/acp-12-1135-2012

Barth, M. C., Bela, M. M., Fried, A., Wennberg, P. O., Crounse, J. D., Clair, J. M. S., et al. (2016). Convective transport and scavenging of peroxides by thunderstorms observed over the central U.S. during DC3. *Journal of Geophysical Research: Atmospheres*, *121*(8), 4272–4295. https://doi.org/10.1002/2015JD024570

Barth, M. C., Cantrell, C. A., Brune, W. H., Rutledge, S. A., Crawford, J. H., Huntrieser, H., et al. (2015). The deep convective clouds and chemistry (DC3) field campaign. *Bulletin of the American Meteorology Society*, *96*(8), 1281–1309. https://doi.org/10.1175/BAMS-D-13-00290.1

Barth, M. C., Kim, S.-W., Skamarock, W. C., Stuart, A. L., Pickering, K. E., & Ott, L. E. (2007). Simulations of the redistribution of formaldehyde, formic acid, and peroxides in the 10 July 1996 Stratospheric-Tropospheric Experiment: Radiation, Aerosols, and Ozone deep convection storm. *Journal of Geophysical Research*, *112*(D13), D13310. https://doi.org/10.1029/2006JD008046

Barth, M. C., Kim, S.-W., Wang, C., Pickering, K. E., Ott, L. E., Stenchikov, G., et al. (2007). Cloud-scale model intercomparison of chemical constituent transport in deep convection. *Atmospheric Chemistry and Physics*, *7*(18), 4709–4731. https://doi.org/10.5194/acp-7-4709-2007

Bela, M. M., Barth, M. C., Toon, O. B., Fried, A., Homeyer, C. R., Morrison, H., et al. (2016). Wet scavenging of soluble gases in DC3 deep convective storms using WRF-Chem simulations and aircraft observations. *Journal of Geophysical Research: Atmospheres*, *121*(8), 4233–4257. https://doi.org/10.1002/2015JD024623

Bela, M. M., Barth, M. C., Toon, O. B., Fried, A., Ziegler, C., Cummings, K. A., et al. (2018). Effects of scavenging, entrainment, and aqueous chemistry on peroxides and formaldehyde in deep convective outflow over the central and Southeast United States. *Journal of Geophysical Research: Atmospheres*, *123*(14), 7594–7614. https://doi.org/10.1029/2018JD028271

Borbon, A., Gilman, J. B., Kuster, W. C., Grand, N., Chevaillier, S., Colomb, A., et al. (2013). Emission ratios of anthropogenic volatile organic compounds in northern mid-latitude megacities: Observations versus emission inventories in Los Angeles and Paris. *Journal of Geophysical Research: Atmospheres*, *118*(4), 2041–2057. https://doi.org/10.1002/jgrd.50059

Bozem, H., Pozzer, A., Harder, H., Martinez, M., Williams, J., Lelieveld, J., & Fischer, H. (2017). The influence of deep convection on HCHO and H_2O_2 in the upper troposphere over Europe. *Atmospheric Chemistry and Physics*, *17*(19), 11835–11848. https://doi.org/10.5194/acp-17-11835-2017

Buchholz, R. R., Emmons, L. K., Tilmes, S., & The CESM2 Development Team, (2019). CESM2.1/CAM-chem instantaneous output for boundary conditions [Dataset]. UCAR/NCARAtmospheric. https://doi.org/10.5065/NMP7-EP60

Cazorla, M., Wolfe, G. M., Bailey, S. A., Swanson, A. K., Arkinson, H. L., & Hanisco, T. F. (2015). A new airborne laser-induced fluorescence instrument for in situ detection of formaldehyde throughout the troposphere and lower stratosphere. *Atmospheric Measurement Techniques*, *8*(2), 541–552. https://doi.org/10.5194/amt-8-541-2015

Chan, K. R., Dean-Day, J., Bowen, S. W., & Bui, T. P. (1998). Turbulence measurements by the DC-8 meteorological measurement system. *Geophysical Research Letters*, *25*(9), 1355–1358. https://doi.org/10.1029/97GL03590

Chen, G. (2013). SEAC4RS, studies of emissions and atmospheric composition, clouds and climate coupling by regional Surveys data archive [Dataset]. National Aeronautics and Space Administration. https://doi.org/10.5067/Aircraft/SEAC4RS/Aerosol-TraceGas-Cloud

Clarke, A., & Kapustin, V. (2010). Hemispheric aerosol vertical profiles: Anthropogenic impacts on optical depth and cloud nuclei. *Science*, *329*(5998), 1488–1492. PMID: 20847262. https://doi.org/10.1126/science.1188838

Clarke, A. D. (1993). Atmospheric nuclei in the Pacific midtroposphere: Their nature, concentration, and evolution. *Journal of Geophysical Research*, *98*(D11), 20633–20647. https://doi.org/10.1029/93JD00797

Crounse, J. D., McKinney, K. A., Kwan, A. J., & Wennberg, P. O. (2006). Measurement of gas-phase hydroperoxides by chemical ionization mass spectrometry. *Analytical Chemistry*, *78*(19), 6726–6732. https://doi.org/10.1021/ac0604235

Cuchiara, G. C., Fried, A., Barth, M. C., Bela, M., Homeyer, C. R., Gaubert, B., et al. (2020). Vertical transport, entrainment, and scavenging processes affecting trace gases in a modeled and observed SEAC4RS case study. *Journal of Geophysical Research: Atmospheres*, *125*(11), e2019JD031957. https://doi.org/10.1029/2019JD031957

DeMott, P. J., Prenni, A. J., Liu, X., Kreidenweis, S. M., Petters, M. D., Twohy, C. H., et al. (2010). Predicting global atmospheric ice nuclei distributions and their impacts on climate. *Proceedings of the National Academy of Sciences of the United States of America*, *107*(25), 11217–11222. https://doi.org/10.1073/pnas.0910818107

Dickerson, R. R., Huffman, G. J., Luke, W. T., Nunnermacker, L. J., Pickering, K. E., Leslie, A. C. D., et al. (1987). Thunderstorms: An important mechanism in the transport of air pollutants. *Science*, *235*(4787), 460–465. https://doi.org/10.1126/science.235.4787.460

DiGangi, E. A., MacGorman, D. R., Ziegler, C. L., Betten, D., Biggerstaff, M., Bowlan, M., & Potvin, C. K. (2016). An overview of the 29 May 2012 Kingfisher supercell during DC3. *Journal of Geophysical Research: Atmospheres*, *121*(24), 14316–14343. https://doi.org/10.1002/2016JD025690

Easter, R. C., & Hales, J. M. (1983). Interpretations of the OSCAR data for reactive gas scavenging. In H. R. Pruppacher, R. G. Semonin, & W. G. N. Slinn (Eds.), *Precipitation scavenging, dry deposition, and resuspension* (pp. 649–662). Elsevier.

Franco, B., Blumenstock, T., Cho, C., Clarisse, L., Clerbaux, C., Coheur, P. F., et al. (2021). Ubiquitous atmospheric production of organic acids mediated by cloud droplets. *Nature*, *593*(7858), 233–237. https://doi.org/10.1038/s41586-021-03462-x

Fried, A., Barth, M. C., Bela, M., Weibring, P., Richter, D., Walega, J., et al. (2016). Convective transport of formaldehyde to the upper troposphere and lower stratosphere and associated scavenging in thunderstorms over the central United States during the 2012 DC3 study. *Journal of Geophysical Research: Atmospheres*, *121*(12), 7430–7460. https://doi.org/10.1002/2015JD024477

Giangrande, S. E., Collis, S., Straka, J., Protat, A., Williams, C., & Krueger, S. (2013). A summary of convective-core vertical velocity properties using ARM UHF wind profilers in Oklahoma. *Journal of Applied Meteorology and Climatology*, *52*(10), 2278–2295. https://doi.org/10.1175/jamc-d-12-0185.1

Grell, G. A., Peckham, S. E., Schmitz, R., McKeen, S. A., Frost, G., Skamarock, W. C., & Eder, B. (2005). Fully coupled "online" chemistry within the WRF model. *Atmospheric Environment*, *39*(37), 6957–6975. https://doi.org/10.1016/j.atmosenv.2005.04.027

Homeyer, C. R., & Bowman, K. P. (2017). Algorithm description document for version 3.1 of the three-dimensional gridded NEXRAD WSR-88D radar (GridRad). [Dataset Technical Report]. University of Oklahoma. http://gridrad.org/pdf/GridRad-v3.1-Algorithm-Description.pdf

Hong, S. Y., & Lim, J. O. J. (2006). The WRF single–moment 6–class microphysics scheme (WSM6). *Journal of the Korean Meteorological Society*, *42*, 129–151.

Hudman, R. C., Jacob, D. J., Turquety, S., Leibensperger, E. M., Murray, L. T., Wu, S., et al. (2007). Surface and lightning sources of nitrogen oxides over the United States: Magnitudes, chemical evolution, and outflow. *Journal of Geophysical Research*, *112*(D12), D12S05. https://doi.org/10.1029/2006JD007912

Hudson, J. G. (1993). Cloud condensation nuclei near marine cumulus. *Journal of Geophysical Research*, *98*(D2), 2693–2702. https://doi.org/10.1029/92JD02169

Huey, L. G., Villalta, P. W., Dunlea, E. J., Hanson, D. R., & Howard, C. J. (1996). Reactions of CF_3O- with atmospheric trace gases. *Journal of Physical Chemistry*, *100*(1), 190–194. https://doi.org/10.1021/jp951928u

Jost, A., Szakáll, M., Diehl, K., Mitra, S. K., & Borrmann, S. (2017). Chemistry of riming: The retention of organic and inorganic atmospheric trace constituents. *Atmospheric Chemistry and Physics*, *17*(16), 9717–9732. https://doi.org/10.5194/acp-17-9717-2017

Lawson, P., Gurganus, C., Woods, S., & Bruintjes, R. (2017). Aircraft observations of cumulus microphysics ranging from the tropics to midlatitudes: Implications for a "new" secondary ice process. *Journal of the Atmospheric Sciences*, *74*(9), 2899–2920. https://doi.org/10.1175/jas-d-17-0033.1

Lawson, R. P. (2011). Effects of ice particles shattering on the 2D-S probe. *Atmospheric Measurement Techniques*, 4(7), 1361–1381. https://doi.org/10.5194/amt-4-1361-2011

Lawson, R. P., Stewart, R. E., & Angus, L. J. (1998). Observations and numerical simulations of the origin and development of very large snowflakes. *Journal of the Atmospheric Sciences*, *55*(21), 3209–3229. https://doi.org/10.1175/1520-0469(1998)055<3209:OANSOT>2.0.CO;2

Leriche, M., Pinty, J.-P., Mari, C., & Gazen, D. (2013). A cloud chemistry module for the 3-D cloud-resolving mesoscale model Meso-NH with application to idealized cases. *Geoscientific Model Development*, *6*(4), 1275–1298. https://doi.org/10.5194/gmd-6-1275-2013

Lucas, C., Zipser, E. J., & Lemone, M. A. (1994). Vertical velocity in oceanic convection off tropical Australia. *Journal of the Atmospheric Sciences*, *51*(21), 3183–3193. https://doi.org/10.1175/1520-0469(1994)051<3183:VVIOCO>2.0.CO;2

Martini, M., Allen, D. J., Pickering, K. E., Stenchikov, G. L., Richter, A., Hyer, E. J., & Loughner, C. P. (2011). The impact of North American anthropogenic emissions and lightning on long-range transport of trace gases and their export from the continent during summers 2002 and 2004. *Journal of Geophysical Research*, *116*(D7), D07305. https://doi.org/10.1029/2010JD014305

Moore, R. H., Karydis, V. A., Capps, S. L., Lathem, T. L., & Nenes, A. (2013). Droplet number uncertainties associated with CCN: An assessment using observations and a global model adjoint. *Atmospheric Chemistry and Physics*, *13*(8), 4235Â–4251. https://doi.org/10.5194/acp-13-4235-2013

Morrison, H., Thompson, G., & Tatarskii, V. (2009). Impact of cloud microphysics on the development of trailing stratiform precipitation in a simulated squall line: Comparison of one- and two-moment schemes. *Monthly Weather Review*, *137*(3), 991–1007. https://doi.org/10.1175/2008MWR2556.1

Müller, J. F., Peeters, J., & Stavrakou, T. (2021). *On the formation of formic acid from formaldehyde processing in liquid clouds*. IGAC Poster CCMI-57C Retrieved from https://www.essoar.org/pdfjs/10.1002/essoar.10507986.1

National Centers for Environmental Prediction/National Weather Service/NOAA/U.S. Department of Commerce. (2005), updated monthly. NCEP north American regional reanalysis (NARR) [Dataset]. Research Data Archive at the National Center for Atmospheric Research, Computational and Information Systems Laboratory. Retrieved from https://rda.ucar.edu/datasets/ds608.0/

Neu, J. L., & Prather, M. J. (2012). Toward a more physical representation of precipitation scavenging in global chemistry models: Cloud overlap and ice physics and their impact on tropospheric ozone. *Atmospheric Chemistry and Physics*, *12*(7), 3289–3310. https://doi.org/10.5194/acp-12-3289-2012

No author (n/d). Sounding data provided by the University of Wyoming-department of atmospheric science [Dataset]. University of Wyoming. Retrieved Januray 19, 2020, from http://weather.uwyo.edu/upperair/sounding.html

NOAA National Weather Service (NWS) Radar Operations Center. (1991). NOAA next generation radar (NEXRAD) level 2 base data [Dataset]. NOAA National Centers for Environmental Information. https://doi.org/10.7289/V5W9574V

Pickering, K. E., Thompson, A. M., Scala, J. R., Tao, W.-K., Dickerson, R. R., & Simpson, J. (1992). Free tropospheric ozone production following entrainment of urban plumes into deep convection. *Journal of Geophysical Research*, *97*(D16), 17985–18000. https://doi.org/10.1029/92JD01716

Radke, L. F., & Hobbs, P. V. (1991). Humidity and particle fields around some small cumulus clouds. *Journal of the Atmospheric Sciences*, *48*(9), 1190–1193. https://doi.org/10.1175/1520-0469(1991)048<1190:hapfas>2.0.co;2

Richter, D., Weibring, P., Walega, J. G., Fried, A., Spuler, S. M., & Taubman, M. S. (2015). Compact highly sensitive multi-species airborne-mid-IR spectrometer. *Applied Physics B: Lasers and Optics*, *119*(1), 119–131. https://doi.org/10.1007/s00340-015-6038-8

Sachse, G. W., Hill, G. F., Wade, L. O., & Perry, M. G. (1987). Fast-response, high-precision carbon monoxide sensor using a tunable diode laser absorption technique. *Journal of Geophysical Research*, *92*(D2), 2071–2081. https://doi.org/10.1029/JD092iD02p02071

Sadowy, G. A., Berkun, A. C., Chun, W., Im, E., & Durden, S. L. (2003). Development of an advanced airborne precipitation radar. (technical feature) [WWW document]. *Microwave Journal*, *46*(1), 84–86.

Skamarock, C., Klemp, B., Dudhia, J., Gill, O., Barker, D., Duda, G., et al., (2008). A description of the advanced research WRF version 3 [software]. University Corporation for Atmospheric Research. https://doi.org/10.5065/D68S4MVH

Snider, J. R., & Huang, J. (1998). Factors influencing the retention of hydrogen peroxide and molecular oxygen in rime ice. *Journal of Geophysical Research*, *103*(D1), 1405–1415. https://doi.org/10.1029/97JD02847

St.Clair, J. M., McCabe, D. C., Crounse, J. D., Steiner, U., & Wennberg, P. O. (2010). Chemical ionization tandem mass spectrometer for the in situ measurement of methyl hydrogen peroxide. *Review of Scientific Instruments*, *81*(9), 094102. https://doi.org/10.1063/1.3480552

Stuart, A. L., & Jacobson, M. Z. (2004). Chemical retention during dry growth riming. *Journal of Geophysical Research*, *109*(D7), D07305. https://doi.org/10.1029/2003JD004197

Stuart, A. L., & Jacobson, M. Z. (2006). A numerical model of the partitioning of trace chemical solutes during drop freezing. *Journal of Atmospheric Chemistry*, *53*(1), 13–42. https://doi.org/10.1007/s10874-006-0948-0

Thompson, A. M., Pickering, K. E., Dickerson, R. R., Ellis, W. G., Jacob, D. J., Scala, J. R., et al. (1994). Convective transport over the central United States and its role in regional CO and ozone budgets. *Journal of Geophysical Research*, *99*(D9), 18703–18711. https://doi.org/10.1029/94JD01244

Thompson, G., Field, P. R., Rasmussen, R. M., & Hall, W. D. (2008). Explicit forecasts of winter precipitation using an improved bulk microphysics scheme. Part II: Implementation of a new snow parameterization. *Monthly Weather Review*, *136*(12), 5095–5115. https://doi.org/10.1175/2008MWR2387.1

Toon, O. B., Maring, H., Dibb, J., Ferrare, R., Jacob, D. J., Jensen, E. J., et al. (2016). Planning, implementation, and scientific goals of the studies of emissions and atmospheric composition, clouds and climate coupling by regional Surveys (SEAC4RS) field mission. *Journal of Geophysical Research: Atmospheres*, *121*(9), 4967–5009. https://doi.org/10.1002/2015JD024297

Twohy, C. H., Clement, C. F., Gandrud, B. W., Weinheimer, A. J., Campos, T. L., Baumgardner, D., et al. (2002). Deep convection as a source of new particles in the midlatitude upper troposphere. *Journal of Geophysical Research*, *107*(D21), AAC6-1–AAC6-10. https://doi.org/10.1029/2001JD000323

Vay, S. A., Choi, Y., Vadrevu, K. P., Blake, D. R., Tyler, S. C., Wisthaler, A., et al. (2011). Patterns of CO_2 and radiocarbon across high northern latitudes during International Polar Year 2008. *Journal of Geophysical Research*, *116*(D14), 116. https://doi.org/10.1029/2011JD015643

Voisin, D., Legrand, M., & Chaumerliac, N. (2000). Scavenging of acidic gases (HCOOH, CH_3COOH, HNO_3, HCl, and SO_2) and ammonia in mixed liquid-solid water clouds at the Puy de Dôme mountain (France). *Journal of Geophysical Research*, *105*(D5), 6817–6835. https://doi.org/10.1029/1999JD900983

von Blohn, N., Diehl, K., Mitra, S. K., & Borrmann, S. (2011). Wind tunnel experiments on the retention of trace gases during riming: Nitric acid, hydrochloric acid, and hydrogen peroxide. *Atmospheric Chemistry and Physics*, *11*(22), 11569–11579. https://doi.org/10.5194/acp-11-11569-2011

von Blohn, N., Diehl, K., Nölscher, A., Jost, A., Mitra, S. K., & Borrmann, S. (2013). The retention of ammonia and sulfur dioxide during riming of ice particles and dendritic snow flakes: Laboratory experiments in the Mainz vertical wind tunnel. *Journal of Atmospheric Chemistry*, *70*(2), 131–150. https://doi.org/10.1007/s10874-013-9261-x

Williams, E., & Stanfill, S. (2002). The physical origin of the land–ocean contrast in lightning activity. *Comptes Rendus Physique*, *3*(10), 1277–1292. https://doi.org/10.1016/S1631-0705(02)01407-X

References From the Supporting Information

Bahreini, R., Ahmadov, R., McKeen, S. A., Vu, K. T., Dingle, J. H., Apel, E. C., et al. (2018). Sources and characteristics of summertime organic aerosol in the Colorado front range: Perspective from measurements and WRF-Chem modeling. *Atmospheric Chemistry and Physics*, *18*, 8293–8312. https://doi.org/10.5194/acp-18-8293-2018

Burkholder, J. B., Sander, S. P., Abbatt, J. P. D., Barker, J. R., Cappa, C., Crounse, J. D., et al. (2019). *Chemical Kinetics and Photochemical Data for Use in Atmospheric Studies, Evaluation No. 19*, JPL Publication 19-5, Jet Propulsion Laboratory. http://jpldataeval.jpl.nasa.gov

Iacono, M. J., Delamere, J. S., Mlawer, E. J., Shephard, M. W., Clough, S. A., & Collins, W. D., (2008). Radiative forcing by long-lived greenhouse gases: Calculations with the AER radiative transfer models. *Journal of Geophysical Research*, *113*(D13), D13103. https://doi.org/10.1029/2008JD009944

Kain, J. S. (2004). The Kain–Fritsch Convective Parameterization: An update. *Journal of Applied Meteorology*, *43*(1), 170–181. https://doi.org/10.1175/1520-0450(2004)043<0170:TKCPAU>2.0.CO;2

McDonald, B. C., McKeen, S. A., Cui, Y. Y., Ahmadov, R., Kim, S.-W., Frost, G. J., et al. (2018). Modeling ozone in the Eastern U.S. using a fuel-based mobile source emissions inventory. *Environmental Science & Technology*, *52*(13), 7360–7370. https://doi.org/10.1021/acs.est.8b00778

Pfister, G. G., Avise, J., Wiedinmyer, C., Edwards, D. P., Emmons, L. K., Diskin, G. D., et al., (2011). CO source contribution analysis for California during ARCTAS-CARB. *Atmospheric Chemistry and Physics*, *11*(15), 7515–7532. https://doi.org/10.5194/acp-11-7515-2011

Tewari, M., Chen, F., Wang, W., Dudhia, J., LeMone, M. A., Mitchell, K., et al. (2004). Implementation and verification of the unified NOAH land-surface model in the WRF model. *Paper presented at 20th conference on weather analysis and Forecasting/16th conference on numerical weather prediction*. (Vol. 1115(6), pp. 2165–2170). American Meteorological Society.

Wiedinmyer, C., Akagi, S. K., Yokelson, R. J., Emmons, L. K., Al-Saadi, J. A., Orlando, J. J., & Soja, A. J. (2011). The fire INventory from NCAR (FINN): A high resolution global model to estimate the emissions from open burning. *Geoscientific Model Development*, *4*(3), 625–641. https://doi.org/10.5194/gmd-4-625-2011